Biomedicine & Pharmacotherapy 164 (2023) 114956

Contents lists available at ScienceDirect

Biomedicine & Pharmacotherapy

journal homepage: www.elsevier.com/locate/biopha

Natural deletion of mouse carboxylesterases *Ces1c/d/e* impacts drug metabolism and metabolic syndrome development

Changpei Gan [a], Jing Wang [a], Yaogeng Wang [a], Alejandra Martínez-Chávez [a,b], Michel Hillebrand [b], Niels de Vries [b], Joke Beukers [b], Maria C. Lebre [a], Els Wagenaar [a], Hilde Rosing [b], Sjoerd Klarenbeek [d], Onno B. Bleijerveld [e], Ji-Ying Song [d], Maarten Altelaar [e,f], Jos H. Beijnen [a,b,c], Alfred H. Schinkel [a,*]

[a] *Division of Pharmacology, The Netherlands Cancer Institute, Amsterdam 1066 CX, The Netherlands*
[b] *Department of Pharmacy & Pharmacology, The Netherlands Cancer Institute, Amsterdam 1066 CX, The Netherlands*
[c] *Division of Pharmacoepidemiology and Clinical Pharmacology, Utrecht Institute for Pharmaceutical Sciences, Utrecht University, Utrecht 3584 CS, the Netherlands*
[d] *Experimental Animal Pathology Facility, The Netherlands Cancer Institute, Amsterdam 1066 CX, The Netherlands*
[e] *Proteomics Core Facility, The Netherlands Cancer Institute, Amsterdam 1066 CX, The Netherlands*
[f] *Biomolecular Mass Spectrometry and Proteomics, Bijvoet Center for Biomolecular Research and Utrecht Institute for Pharmaceutical Sciences, University of Utrecht, and Netherlands Proteomics Center, Padualaan 8, Utrecht 3584 CH, The Netherlands*

ARTICLE INFO

Keywords:
Ces1 enzymes
Irinotecan
Capecitabine
Obesity
Acute phase response
Inflammation

ABSTRACT

Mammalian carboxylesterase 1 enzymes can hydrolyze many xenobiotic chemicals and endogenous lipids. We here identified and characterized a mouse strain (FVB/NKI) in which three of the eight *Ces1* genes were spontaneously deleted, removing *Ces1c* and *Ces1e* partly, and *Ces1d* entirely. We studied the impact of this *Ces1c/d/e* deficiency on drug and lipid metabolism and homeostasis. *Ces1c/d/e*$^{-/-}$ mice showed strongly impaired conversion of the anticancer prodrug irinotecan to its active metabolite SN-38 in plasma, spleen and lung. Plasma hydrolysis of the oral anticancer prodrug capecitabine to 5-DFCR was also profoundly reduced in *Ces1c/d/e*$^{-/-}$ mice. Our findings resolved previously unexplained FVB/NKI pharmacokinetic anomalies. On a medium-fat diet, *Ces1c/d/e*$^{-/-}$ female mice exhibited moderately higher body weight, mild inflammation in gonadal white adipose tissue (gWAT), and increased lipid load in brown adipose tissue (BAT). *Ces1c/d/e*$^{-/-}$ males showed more pronounced inflammation in gWAT and an increased lipid load in BAT. On a 5-week high-fat diet exposure, *Ces1c/d/e* deficiency predisposed to developing obesity, enlarged and fatty liver, glucose intolerance and insulin resistance, with severe inflammation in gWAT and increased lipid load in BAT. Hepatic proteomics analysis revealed that the acute phase response, involved in the dynamic cycle of immunometabolism, was activated in these *Ces1c/d/e*$^{-/-}$ mice. This may contribute to the obesity-related chronic inflammation and adverse metabolic disease in this strain. While *Ces1c/d/e* deficiency clearly exacerbated metabolic syndrome development, long-term (18-week) high-fat diet exposure overwhelmed many, albeit not all, observed phenotypic differences.

1. Introduction

Mammalian carboxylesterase 1 (Ces1/CES1) enzymes are serine hydrolases which can hydrolyze carboxylic acid ester, amide, and thioester bonds in many substrates. Ces1/CES1 enzymes detoxify various drugs, nerve agents, and environmental pollutants, and activate some prodrugs [1]. Endogenous lipids such as triglycerides, cholesteryl and retinyl esters can also be hydrolyzed by Ces1/CES1, thus influencing lipid homeostasis [2].

The mouse carboxylesterase 1 (*Ces1*) gene locus harbors eight individual *Ces1* genes (*Ces1a* to *Ces1h*). These genes show quite broad tissue distributions and distinct functions [3]. For example, mouse *Ces1c* is highly expressed in liver and predominantly secreted into plasma due to lack of an endoplasmic reticulum (ER) retention sequence. This presents an important species difference between mouse and human as the essentially single human CES1 protein contains an ER retention signal and is retained in liver. The mouse plasma Ces1c enzyme impacts hydrolysis of the anti-cancer prodrug irinotecan to its active metabolite

* Correspondence to: Division of Pharmacology, The Netherlands Cancer Institute, Plesmanlaan 121, 1066 CX Amsterdam, The Netherlands.
E-mail address: a.schinkel@nki.nl (A.H. Schinkel).

https://doi.org/10.1016/j.biopha.2023.114956
Received 3 March 2023; Received in revised form 12 May 2023; Accepted 27 May 2023
Available online 31 May 2023

SN-38 [4,5]. In earlier studies, we demonstrated that mouse Ces1c increases cabazitaxel and everolimus plasma exposure, likely by tightly binding and stabilizing these drugs in blood [6,7]. Ces1d has been shown in vitro to stimulate fatty acid efflux from adipocytes [8], and global knockout of *Ces1d* in mice has been reported to reduce blood lipids and improve glucose tolerance compared with wild-type (WT) controls [9]. Adding to its functional complexity, Ces1d appears to have distinct functional effects in different tissues: liver-specific *Ces1d* knockout mice showed decreased blood lipids without fatty liver [10]; but adipose-tissue-specific deficiency of *Ces1d* led to obesity-related metabolic disorders (liver steatosis, type 2 diabetes) [11]. The less well-studied Ces1e is a potent retinyl ester hydrolase which is highly expressed in liver and plays a role in retinoid metabolism in vitro [12].

Obesity-related metabolic diseases (nonalcoholic fatty liver disease, type 2 diabetes mellitus, cardiovascular disease, etc.) are increasingly becoming a global health issue [13,14]. Chronic inflammation in metabolic tissues is a well-recognized and widely accepted feature of obesity, which plays crucial roles in the genesis of obesity-related metabolic disease [15,16]. In the initial stage, various triggers (ER stress, mitochondrial dysfunction, hypoxia, and lipotoxicity) can activate proinflammatory pathways in lipid-metabolizing organs. Both innate and adaptive immune cells are attracted by sensing chemokines secreted from these inflamed tissues, and further exacerbate metabolic inflammation [17]. As part of the innate immune system, the acute phase response (APR) is an early-defense system which is triggered by different stimuli (infection, trauma, stress and inflammation). The liver then produces many acute phase proteins (serum amyloid A (SAA), hemopexin and complement factors) aiming to reestablish physiological homeostasis [18]. However, if this homeostasis is not achieved, a continued APR can also induce chronic and/or more severe inflammation. This can play key roles in the development of several diseases. For example, SAA promotes Th17-mediated inflammatory diseases [19], stimulates pulmonary allergen-driven type 2 immunity [20], and helps to establish a pro-metastatic niche in the liver [21]. Evidence supporting the important role of the APR in the genesis of metabolic disorders has also emerged [22,23]. Hepatic overexpression of mouse Saa1 further directly aggravates hepatitis development in a mouse model [24].

In this study we identified a natural genomic deletion covering part of *Ces1c*, the whole of *Ces1d*, and part of *Ces1e* in an FVB(NKI) substrain previously considered wild-type. To understand the impact of this mutation on pharmacological and physiological processes in vivo, pharmacokinetic studies of two anticancer prodrugs (irinotecan and capecitabine) were performed. We also investigated lipid metabolism and several metabolic-syndrome related phenotypes in *Ces1c/d/e*$^{-/-}$ mice under medium- and high-fat diet conditions, respectively.

2. Material and methods

2.1. Animals

The mice were fed with a medium-fat diet with 24% kcal from fat (801228, Special Diets Services, Essex, UK) or with a high-fat diet with 60% kcal from fat (820349, Special Diets Services, Essex, UK). They were housed in 12-hour light/12-hour dark cycle under controlled temperature. Wild type (FVB/NRj) and *Ces1c/d/e*$^{-/-}$ (FVB/NKI) mice with comparable genetic strain background (FVB) were used in this study (3–24 weeks).

2.2. Historical reconstruction of the Ces1c/d/e deletion in FVB/NKI mice

Insights from the current study have allowed us to reconstruct what must have occurred in our animal facility, although we lack the historical mouse samples to prove all elements of this reconstruction. The original FVB/N (subsequently called FVB/NKI) strain obtained some 30 years ago must have been *Ces1c/d/e* proficient. Over the years, two separate breeding stocks of this strain were maintained, one, the central breeding stock, primarily by brother-sister crossings, the other by random breeding. At some time, perhaps 10 or 15 years ago, the spontaneous *Ces1c/d/e* deletion must have occurred in the central breeding stock. It was then coincidentally fixed to homozygosity by the systematic brother-sister crossings. The other random breeding population remained *Ces1c/d/e* proficient. This proficient FVB/NKI population was used to cross back most of the various knockout and transgenic strains for other detoxifying genes we generated over the years, and thus nearly all of these strains are homozygously *Ces1c/d/e* proficient. The random-bred wild-type population, however, was at several points later in time replenished from the inbred central breeding stock, and thus developed into a genetically heterogeneous population with mostly homozygous, and some heterozygous *Ces1c/d/e* deletion mice. The homozygous deletion WT mice are everolimus "low", and the heterozygous deletion WT mice are everolimus "high" mice.

2.3. Plasma and tissue pharmacokinetic experiments

Irinotecan hydrochloride trihydrate (20 mg/ml, obtained from Fresenius Kabi, Cheshire, United Kingdom) was diluted with 0.9% w/v of NaCl/water to 5 mg/ml. For oral and i.v. experiments, 4 μl of prepared irinotecan solution per gram of body weight was administered to male mice (n = 4–5). Blood samples were collected from the tail vein at different time points (oral experiment: 7.5 min, 15 min, 30 min, 60 min, 120 min, 240 min; i.v. experiment: 7.5 min, 15 min, 30 min, 60 min, 120 min respectively), using heparinized capillary tubes (Sarstedt, Germany). At 8 h (oral) or 4 h (i.v.), blood was collected by cardiac puncture under isoflurane anesthesia, followed by cervical dislocation. Tissues were harvested and rapidly frozen at −30℃. Blood samples were centrifuged at 2700 g for 6 min at 4 °C, and the plasma fraction was collected and stored at −30 °C until analysis. Tissues were homogenized in 4% (w/v) BSA in water for analysis. Samples were deproteinized by adding a mixture of the organic solvents acetonitrile and methanol (1:1, v/v), using a 4-fold (v/v) solvent excess, followed by vigorous mixing, centrifugation, and collection of supernatants. HPLC-fluorescence was applied to measure irinotecan and SN-38 concentrations in the mouse samples as described previously [25].

The concentration of capecitabine (Carbosynth, Berkshire, UK) working solution was 50 mg/ml, with 3% (v/v) DMSO, 4% Tween 80/ethanol (1:1; v/v) and 40 mM NaAc (pH 4.2). This drug solution was orally gavaged to female mice (n = 4–5) at a volume of 10 μl/g body weight to obtain a dose of 500 mg/kg. The further experimental procedure was as described above for the irinotecan oral experiment. Samples were deproteinized by adding a mixture of the organic solvents acetonitrile and methanol (1:1, v/v), using a 3-fold (v/v) solvent excess, followed by vigorous mixing, centrifugation, and collection of supernatants. HPLC-MS/MS was used to analyze levels of capecitabine and its 4 metabolites (5-DFCR, 5-DFUR, 5-FU and FBAL), as described previously [26].

2.4. Irinotecan/SN-38 toxicity experiment

30 mg/kg irinotecan hydrochloride trihydrate was daily administered to male mice by i.v. injection (n = 4–8) for 6 days. Mouse body weight change and general appearance were monitored daily. For hematologic analysis, blood samples were harvested from the tail vein at day 0 and day 7 (one day before the first irinotecan injection, and 24 h after the last administration), then analyzed by Beckman Colter analyzer. At day 7, mouse thymus, jejunum and sternum were collected for histological assessment.

2.5. Analysis of triglyceride secretion in vivo

Mice were fasted for 16 h, followed by intraperitoneal injection of the lipase inhibitor Poloxamer-407 (Sigma-Aldrich, Steinheim, Germany) in 0.9% NaCl at 1 g/kg body weight to block metabolism of

released triglycerides. Aliquots of tail vein blood were collected at different times, plasma was prepared and triglyceride levels were determined by LabAssay Triglyceride Kit (Wako Chemicals, Osaka, Japan).

2.6. Measurement of plasma and hepatic parameters

Plasma triglyceride, alkaline phosphatase and alanine aminotransferase concentrations were measured by Roche Cobas analyzer. Plasma glycerol and free fatty acid levels were determined by appropriate kits (Products No. 2913 and 3055, Instruchemie, Delfzijl, The Netherlands). To measure hepatic triglyceride level, we first isolated hepatic lipid by Lipid Extraction Kit (PK-CA577-K216, PromoCell, Heidelberg, Germany), and then the hepatic triglyceride concentration was determined by LabAssay Triglyceride Kit (Wako Chemicals, Osaka, Japan).

2.7. Glucose and insulin tolerance tests

Glucose tolerance test was performed by oral administration of glucose monohydrate (Merck, Darmstadt, Germany) (1 g/kg body weight) to mice after a 16-h fast. Blood glucose level was assessed before (t = 0 min) and after oral glucose administration at different time points (15, 30, 60, 90, and 120 min) by ACCU-CHEK Performa glucose meter (Roche Diagnostics, Mannheim, Germany). For the insulin tolerance test, insulin (Sigma-Aldrich, Steinheim, Germany) (0.5 U/kg body weight) was intraperitoneally injected to mice after a 6-h fast, then blood glucose was measured as described for the glucose tolerance test.

2.8. Quantitative Real-time PCR and histologic analysis

We first extracted total RNA from mouse liver and small intestine using RNeasy Mini Kit (QIAGEN GmbH, Hilden, Germany). RNA from mouse white adipose tissue was isolated by RNeasy Lipid Tissue Mini Kit (QIAGEN GmbH, Hilden, Germany). This was followed by cDNA synthesis with Maxima First Strand cDNA Synthesis Kit (Thermo Scientific, Vilnius, Lithuania). Specific primers for mouse *Ces1*, *Ces2*, *Ces3* genes and inflammatory genes were purchased (QIAGEN GmbH, Hilden, Germany), and RT-PCR was performed as described previously [27]. Hematoxylin and eosin (H&E) and lipid staining (Oil Red O) were applied for tissue pathologic analysis as previously described [28].

2.9. Mouse liver proteomics

Mouse liver tissue specimens ($n = 6$) were homogenized and lysed by the T-PER Tissue Protein Extraction Reagent with Pierce™ Protease and Phosphatase Inhibitor Mini Tablets (Thermo Scientific, Waltham, MA, USA). Lysate aliquots comprising 40 μg protein were taken for reduction with 20 mM DTT (20 min, at 55 °C) and alkylation with 40 mM iodoacetamide (30 min, at RT in the dark), after which proteins were digested overnight with trypsin (Sigma-Aldrich; enzyme/substrate ratio 1:10) on S-Trap Micro spin columns according to the manufacturer's instructions (ProtiFi, NY, USA). Peptides were eluted, vacuum dried and stored at −80 °C until LC-MS/MS analysis. LC-MS/MS was performed by nanoLC-MS/MS on an Orbitrap Exploris 480 mass spectrometer (Thermo Scientific, Waltham, MA, USA) connected to a Proxeon nLC1200 system. Peptides were directly loaded onto the analytical column (ReproSil-Pur 120 C18-AQ, 1.9 μm, 75 μm × 500 mm, packed in-house) and eluted in a 90-minutes gradient containing a non-linear increase from 6% to 30% solvent B (solvent A was 0.1% formic acid/water and solvent B was 0.1% formic acid/80% acetonitrile). The Exploris 480 was run in data-independent acquisition (DIA) mode, with full MS resolution set to 120,000 at m/z 200, MS1 mass range was set from 350 to 1400, normalized AGC target was 300% and maximum injection time was 45 ms. DIA was performed on precursors from 400 to 1000 in 48 windows of 13.5 Da with an overlap of 1 Da. Resolution was set to 30,000 and normalized collision energy was 27.

RAW files were analyzed with DIA-NN (version 1.8) [29] using standard settings. Fragment spectra were searched against the Swissprot human database (version 2022_02; 20,375 entries) by selecting 'FASTA digest for library-free search'; Trypsin/P was specified as protease specificity allowing a maximum of 1 miscleavage; N-terminal excision (M) and carbamidomethylation (C) were selected as fixed modifications and match between runs was applied. Protein group abundances were extracted from the DIA-NN result files, imported into Perseus (1.6.15.0) [30] and Log2-transformed. Values were filtered for presence in at least 4 out of 6 samples of either the *Ces1c/d/e* mutant or wild-type (FVB/NRj) mouse group. Missing values were replaced by an imputation-based normal distribution using a width of 0.3 and a downshift of 2.4. Differentially expressed proteins were determined using a multiple testing-corrected *t*-test with s0 value 0.2 and FDR 0.05 as cutoff values.

2.10. Statistics

Two-tailed unpaired Student's *t* test was used to assess the significance of differences between 2 sets of data. Data are presented as mean ± SD, differences were considered to be statistically significant when P was less than 0.05.

2.11. Study approval

The Animal Experiments Review Board of the Netherlands Cancer Institute (complying with Dutch Legislation) approved all mouse experiments (Project numbers: AVD301002016595; AVD3010020174487).

3. Results

3.1. Characterization of a natural deletion covering Ces1c/d/e in FVB/NKI mice

In a separate mouse *Ces1* cluster (*Ces1a* to *Ces1h*) knockout project [31], we checked whether all eight mouse *Ces1* genes were successfully deleted in the knockout strain. FVB/NKI genomic DNA was used as wild-type (WT) positive control in this PCR genotyping. Unexpectedly, we found that the mouse *Ces1d* gene was negative in FVB/NKI mice, whereas a PCR product of *Ces1d* was present in another commonly used WT FVB substrain, FVB/NRj (Fig. 1A, primers shown in Supplemental Table 1). These results suggested that the mouse *Ces1d* gene was possibly lost in the FVB/NKI substrain by natural mutation. Natural DNA mutation (genetic drift) is commonly observed in wild conditions [32], but especially also in inbred laboratory mouse lines [33,34]. To precisely delineate the lost DNA region, we performed DNA sequencing across the mutant allele, and identified the exact location and size of the deletion. This revealed that an approximately 87-kb DNA fragment was homozygously lost in this substrain, containing the entire *Ces1d* gene, part of *Ces1c* (exons 6–1, encoding 265 amino acids) and part of *Ces1e* (exons 14–12, encoding 125 amino acids) (Fig. 1B). As in these *Ces1* genes, one catalytic active-site residue, serine, is encoded in exon 5, and another, histidine, in exon 12 [35], it is reasonable to assume that this FVB/NKI substrain completely lacks the enzymatic activities of *Ces1c*, *Ces1d* and *Ces1e*. We therefore hereafter identify this FVB/NKI substrain as *Ces1c/d/e*$^{-/-}$ mice, with global knockout of the three affected *Ces1* genes. Real-time PCR analysis of RNA expression of the mouse *Ces1* gene family in this substrain in liver revealed markedly downregulated expression of the *Ces1b*, *Ces1c*, *Ces1d* and *Ces1e* genes. Because *Ces1b* RNA is extremely similar to *Ces1c* RNA, it is likely that the RT-PCR primers cross-recognize these two genes. It is therefore possible that the reduced *Ces1b* signal to a large extent reflects the reduced level of (truncated) *Ces1c* RNA. Meanwhile, *Ces1f* and *Ces1g* were moderately upregulated in the liver of *Ces1c/d/e*$^{-/-}$ mice compared with WT (FVB/NRj) controls (Supplemental Table 2). The expression levels of the functionally and structurally related *Ces2* (*Ces2a* to *Ces2h*, except for the pseudogene

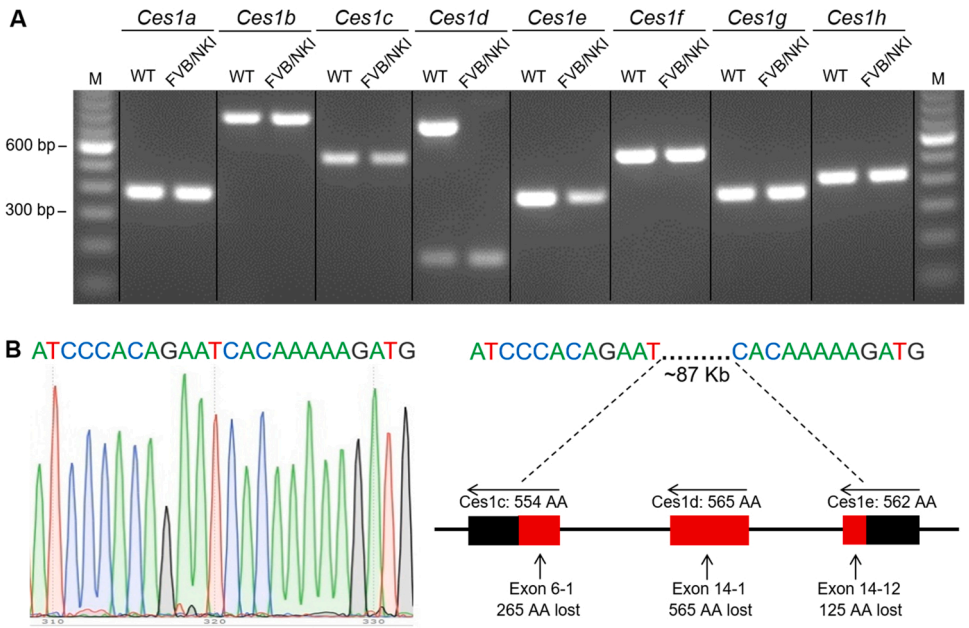

Fig. 1. Characterization of *Ces1c/d/e* natural mutation in FVB/NKI mice. (A) Genomic PCR analysis of all 8 *Ces1* genes in wild type (WT: FVB/NRj) and FVB/NKI mice. (B) DNA sequence across the junction in the mutant allele (between middle T and C), and the profile of the deleted region (red box) in FVB/NKI mice. AA: amino acid.

Ces2d), and *Ces3* (*Ces3a* and *Ces3b*) gene families were also checked: *Ces2b*, *Ces2c* and *Ces3b* were slightly upregulated (Supplemental Table 2). The expression profiles of *Ces1*, *Ces2* and *Ces3* genes were also assessed in small intestine, where roughly similar changes were detected (Supplemental Table 2). *Ces1c/d/e*$^{-/-}$ mice showed a normal life span and no obvious anatomic abnormalities. Physiological studies of this strain mainly focusing on lipid metabolism will be discussed below.

3.2. Mutation of Ces1c/d/e decreases the conversion of irinotecan to SN-38

The anticancer prodrug irinotecan can be hydrolyzed by esterases to its active metabolite, SN-38 [36] (Fig. S1), and is commonly used to treat small cell lung cancer and metastatic colorectal cancer [27]. In a single *Ces1c* mutant mouse model obtained after alkylating agent-mediated mutagenesis, Potter et al. demonstrated that mouse plasma esterase Ces1c (which is abundant in mouse plasma) is responsible for the

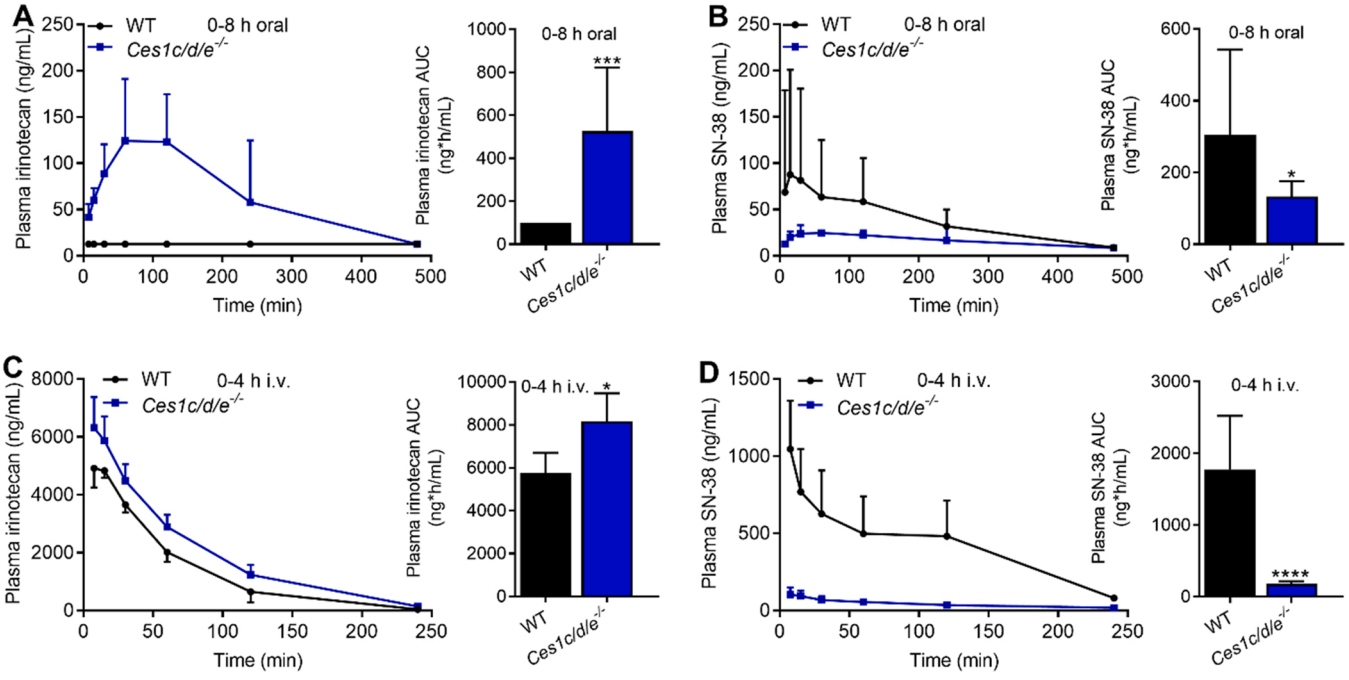

Fig. 2. *Ces1c/d/e*$^{-/-}$ mice show impaired conversion of irinotecan to SN-38 in plasma. Pharmacokinetics of irinotecan and SN-38 after oral or i.v. administration of irinotecan (20 mg/kg) to male WT and *Ces1c/d/e*$^{-/-}$ mice. Plasma concentration versus time curves and AUCs of irinotecan and SN-38 after oral (A-B) or i.v. (C-D) administration. Data are presented as mean ± SD ($n = 4$–5; *$P < 0.05$; ***$P < 0.001$; ****$P < 0.0001$ when compared with WT mice; the statistical calculation was performed after log-transformation of data; two-tailed unpaired Student's *t* test).

hydrolysis of irinotecan to SN-38 in plasma [4,5]. In contrast, in humans carboxylesterase 1 (CES1) is efficiently retained in cells by an endoplasmic reticulum (ER) retention signal, the C-terminal tetrapeptide HXEL [37], which is absent from Ces1c. This species difference makes that WT mice are not an ideal model for pharmacokinetic studies of drugs hydrolyzed by Ces/CES enzymes.

To investigate the pharmacokinetic profile of irinotecan and SN-38 in *Ces1c/d/e*$^{-/-}$ mice, irinotecan (20 mg/kg) was administered orally or i.v. to male WT (FVB/NRj) and mutant mice. HPLC-fluorescence was applied to measure concentrations of irinotecan and SN-38 [25]. The plasma AUCs of irinotecan in *Ces1c/d/e*$^{-/-}$ mice were 5.3- and 1.4-fold higher than those in WT mice (526 ± 296.2 vs $< 99.2 \pm 99.2$ ng*h/ml; $P < 0.001$ and 8167 ± 1303 vs 5754 ± 945 ng*h/ml; $P < 0.05$) after oral and i.v. administration, respectively (Fig. 2A, C and Supplemental Table 3). After oral dosing, irinotecan plasma concentrations were always below the limit of detection (12.5 ng/ml) in WT mice (Fig. 2A), suggesting effective hydrolysis of irinotecan. *Ces1c/d/e*$^{-/-}$ mice appeared to have markedly reduced hydrolysis of irinotecan, and hence increased irinotecan and reduced SN-38 plasma levels. In *Ces1c/d/e*$^{-/-}$ mice, plasma AUCs of SN-38 were at most 44% or even 10% of those seen in WT controls (132.5 ± 43.1 vs 304.1 ± 238.7 ng*h/ml; $P < 0.05$ and 177.1 ± 35.9 vs 1776 ± 747 ng*h/ml; $P < 0.0001$) after oral and i.v. dosing, respectively (Fig. 2B, D and Supplemental Table 3). Systemic plasma SN-38 was moderately but significantly lower after oral dosing in *Ces1c/d/e*$^{-/-}$ compared to WT mice (Fig. 2B), and a more pronounced decrease was seen after i.v. dosing (Fig. 2D). This suggests that both intestine and a non-intestinal compartment participate in irinotecan hydrolysis. When the plasma irinotecan and SN-38 concentrations after i.v. dosing were added up, there was no significant difference between the two strains at any time point (Fig. 2C, D and data not shown). This suggests that the main cause of the differences in the i.v. experiment was the hydrolysis of irinotecan to SN-38, likely primarily in plasma.

Mouse Ces1c/d/e enzymes are also present in several pharmacokinetically relevant organs [3]. To better understand the impact of *Ces1c/d/e* mutation on the distribution and metabolic fate of irinotecan, we analyzed WT and *Ces1c/d/e*$^{-/-}$ male mice 8 h after oral, and 4 h or 10 min after i.v. administration of irinotecan. Irinotecan and SN-38 levels in liver, kidney, spleen, lung, small intestine, small intestinal content and colon were measured. In liver or kidney, we did not observe significant differences in absolute concentrations of irinotecan and SN-38, nor for SN-38-to-irinotecan ratios 8 h after oral and 4 h after i.v. administration between WT and *Ces1c/d/e*$^{-/-}$ mice (Fig. S2A-D). However, significantly lower SN-38 concentration were seen in liver and kidney from *Ces1c/d/e*$^{-/-}$ mice 10 min after i.v. dosing (Fig. S2E, F). This suggests a moderate effect of Ces1c/d/e enzymes on the irinotecan and SN-38 disposition in these two tissues at an early time point. Eight hours after oral dosing, spleen showed higher irinotecan and a reduced SN-38-to-irinotecan ratio in *Ces1c/d/e*$^{-/-}$ mice, but no difference in lung (Fig. S3A, B). However, in the two i.v. experiments (4 h and 10 min), spleen and lung SN-38 concentrations and SN-38-to-irinotecan ratios in *Ces1c/d/e*$^{-/-}$ mice were markedly reduced (Fig. 3A-D), similar patterns were seen in lung (Fig. 3B and D). However, because of the pronounced influence of *Ces1c/d/e* ablation on the plasma levels of irinotecan and SN-38 (Fig. S4), discriminating the tissue-specific and plasma-specific contribution of Ces1c/d/e to the conversion from irinotecan to SN-38 is challenging. We also analyzed levels of irinotecan and SN-38 in the small intestine, small intestinal content (SIC) and colon after the oral and i.v. administrations. No significant differences in absolute concentrations of irinotecan and SN-38, nor for SN-38-to-irinotecan ratios were observed between WT and *Ces1c/d/e*$^{-/-}$ mice (Fig. S5A-H). Only in the 10 min i.v. experiment, the concentration of SN-38 in colon was significantly decreased (Fig. S5I). Four hours after i.v. administration, we detected high concentrations of both irinotecan and SN-38 in the SIC of WT and *Ces1c/d/e*$^{-/-}$ mice (Fig. S5E), demonstrating that these compounds are actively excreted into the intestinal lumen in both mouse strains.

Dose-limiting toxicities of irinotecan restrict its therapeutic use in the clinic [38,39]. To assess and compare irinotecan/SN-38-induced toxicity between *Ces1c/d/e*$^{-/-}$ and WT mice, irinotecan (30 mg/kg) was administered for 6 days (i.v. once daily). Both mouse strains showed a roughly similar drop in bodyweight (Fig. S6A). When comparing the white blood cell (WBC) count between day 0 and day 7, we noticed that *Ces1c/d/e*$^{-/-}$ mice exhibited a comparable reduction of WBC as WT mice (Fig. S6B). Histopathological analysis on day 7 revealed that WT and *Ces1c/d/e*$^{-/-}$ mice both showed marked thymus atrophy (reduction of

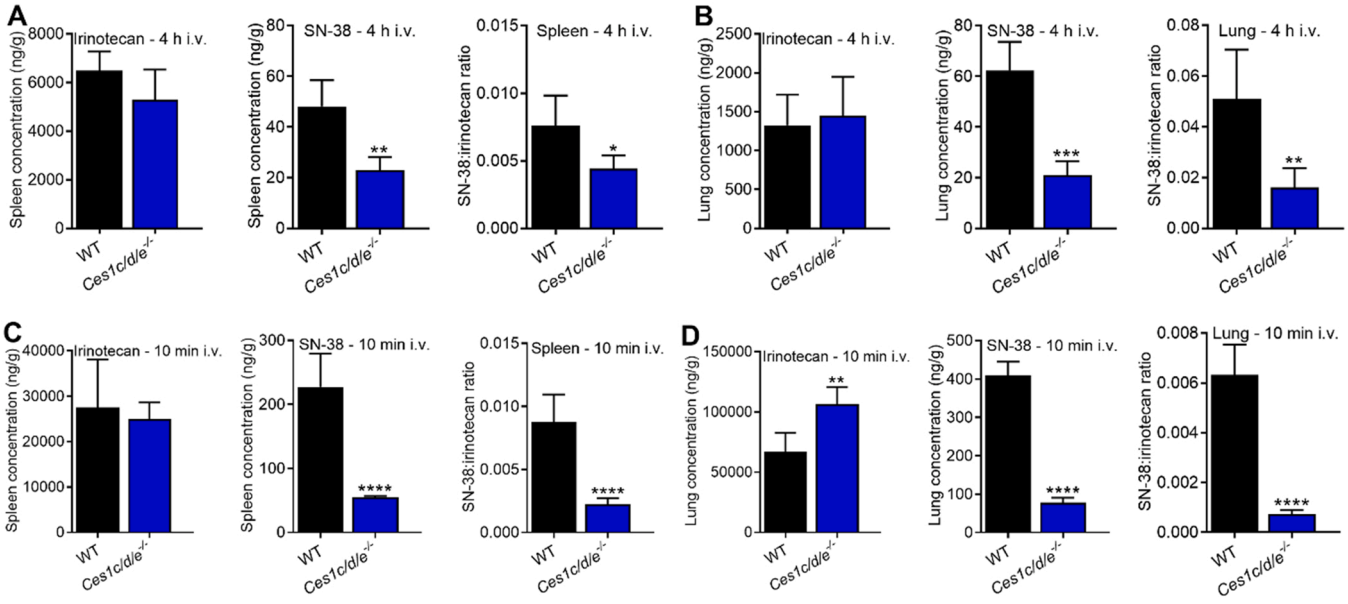

Fig. 3. *Ces1c/d/e*$^{-/-}$ mice exhibit reduced ratios of SN-38 to irinotecan in spleen and lung after i.v. dosing. Tissue concentrations of irinotecan, SN-38 and SN-38-to-irinotecan ratios in spleen and lung after 4 h i.v. (A-B) or 10 min i.v. (C-D) administration of irinotecan (20 mg/kg) to male WT and *Ces1c/d/e*$^{-/-}$ mice. Data are presented as mean ± SD ($n = 4$–5; * $P < 0.05$; ** $P < 0.01$; *** $P < 0.001$; **** $P < 0.0001$ when compared with WT mice; the statistical calculation was performed after log-transformation of data; two-tailed unpaired Student's *t* test).

thymus size), and lymphocytes were severely depleted with extensive thinning of primarily cortex but also medulla compared with WT untreated control (Fig. S6C). In contrast, jejunum structure and sternal bone marrow cell density were relatively similar in these 3 groups (Fig. S6D, E). These results together indicate that loss of Ces1c, 1d and 1e enzymes in mice did not directly affect irinotecan/SN-38 toxicity at this dose, possibly because other Ces enzymes can take over the role of SN-38 formation in these tissues.

3.3. Mutation of *Ces1c/d/e* decreases the metabolite-to-capecitabine ratios in plasma

Capecitabine, an oral fluoropyrimidine (5-FU) carbamate prodrug, is prescribed for metastatic breast and colorectal cancer [26]. The carbamate bond in capecitabine can be hydrolyzed both by human CES1 and CES2, yielding the first metabolite, 5-DFCR, with roughly equal efficiency [40], after which other enzymes catalyze formation of further metabolites, including 5-FU (Fig. S7). We therefore tested whether the conversion from capecitabine to its 4 metabolites (5-DFCR, 5-DFUR, 5-FU and FBAL) may be different in *Ces1c/d/e*$^{-/-}$ mice. Capecitabine (500 mg/kg) was orally administered to female WT and *Ces1c/d/e*$^{-/-}$ mice, and HPLC-MS/MS was applied to quantify the plasma levels of capecitabine and its metabolites over 8 h [26]. The plasma AUC of capecitabine in *Ces1c/d/e*$^{-/-}$ was 45-fold higher than in WT controls (61417 ± 18969 vs 1365 ± 543 ng*h/ml; $P < 0.0001$) (Fig. 4A, B and Supplemental Table 4). Correspondingly, the plasma AUC for the first metabolite, 5-DFCR, was 29% lower than that in WT mice (154421 ± 25494 vs 217117 ± 24764 ng*h/ml; $P < 0.01$) (Fig. 4C, D and Supplemental Table 4). This demonstrates that loss of *Ces1c/d/e* enzymes in mice has a substantial impact on the absolute concentrations of capecitabine and 5-DFCR in plasma. In contrast, the plasma AUCs for the other 3 metabolites (5-DFUR, 5-FU and FBAL) were quite similar between these two strains (Fig. 4E-J). We further calculated the plasma metabolite-to-capecitabine ratios. The plasma AUC ratio of 5-DFCR-to--capecitabine of *Ces1c/d/e*$^{-/-}$ was 98.5% lower than that in WT mice (2.7 ± 0.8 vs 185.4 ± 91.8; $P < 0.0001$) (Fig. S8A, B and Supplemental Table 4). The metabolite-to-capecitabine ratios of the other three metabolites showed similar profiles of differences, although they were primarily caused by the difference in plasma concentrations of capecitabine (Fig. S8C-H, Supplemental Table 4). Together, these data illustrate that mouse *Ces1c/d/e* enzymes can influence the pharmacokinetics of capecitabine and related metabolites in plasma.

We also measured capecitabine and metabolite concentrations in various tissues (liver, kidney, spleen, lung, SI, SIC and colon) at 8 h. At this relatively late time point, where most compounds had been cleared from plasma, no significant differences in most tissue concentrations were detected (Fig. S9). It should be noted that, in spite of the strong influence of *Ces1c/d/e* enzymes on plasma levels of capecitabine and 5-DFCR, the 5-FU concentrations in plasma and tissues were not markedly changed in the *Ces1c/d/e*$^{-/-}$ strains (Fig. 4G, H and Fig. S9). It thus appears that there are adequate alternative conversion routes from capecitabine to DFCR to still generate similar amounts of 5-DFUR and 5-FU in the body.

3.4. *Ces1c/d/e* mutation disrupts lipid homeostasis in adipose tissues under a medium-fat diet

It has been reported that loss of *Ces1d* in mice can decrease blood lipids and upregulate energy expenditure [9]. To further study the physiological functions of mouse Ces1 enzymes, we analyzed WT and *Ces1c/d/e*$^{-/-}$ mice kept on a medium-fat diet (24% energy from fat). At 12–13 weeks, both strains showed comparable body weights (Fig. S10A). When body weight development was monitored from 6 to 15 weeks, *Ces1c/d/e*$^{-/-}$ female mice displayed mildly but significantly higher body weights compared with WT controls (Fig. 5A). This corresponded with significantly elevated weights of mesenteric white adipose tissue (mWAT), retroperitoneal white adipose tissue (rWAT), and perhaps perigonadal white adipose tissue (gWAT), and inguinal white adipose tissue (iWAT), but not interscapular brown adipose tissue (iBAT) (Fig. 5C) [41]. Male *Ces1c/d/e*$^{-/-}$ mice showed similar body weight development and adipose tissue weights as WT controls (Fig. 5B, D). For both females and males, other organ weights (liver, kidney, spleen, lung, heart) were comparable (Fig. S10B-C). Histological analysis (haematoxylin and eosin (H&E) staining) indicated that average gWAT adipocyte size was markedly increased, with mild immune cell infiltration in *Ces1c/d/e*$^{-/-}$ females. In *Ces1c/d/e*$^{-/-}$ males, even though the average gWAT adipocyte size was only slightly increased, there was markedly increased inflammation in gWAT (steatitis) compared to WT mice (Fig. 5E). Moreover, H&E staining of iBAT revealed somewhat increased lipid deposition primarily by an increased number of cytoplasmic large lipid vacuoles in *Ces1c/d/e*$^{-/-}$ compared to WT mice in both females and males (Fig. 5F).

Both global and liver-specific ablation of *Ces1d* can reduce plasma triglyceride levels by attenuating VLDL (very low-density lipoprotein) secretion from liver to blood [9,10]. However, plasma triglyceride levels were not markedly changed in *Ces1c/d/e*$^{-/-}$ mice compared to WT controls (Fig. S11A), nor was the dynamic process of triglyceride secretion from liver to blood (Fig. S11B-C). Also the liver morphology as assessed by H&E staining, and neutral lipid staining level with Oil Red O were very similar between WT and *Ces1c/d/e*$^{-/-}$ mice (Fig. S11D and E). Taken together these data indicate that, under a medium-fat diet, mouse *Ces1c/d/e* deficiency affects the regulation of lipid homeostasis in adipose tissues, but does not have a detectable impact on triglyceride homeostasis in blood and liver.

3.5. *Ces1c/d/e* mutation predisposes mice to developing obesity with severely disrupted lipid homeostasis under a high-fat diet

Deficiencies in lipid homeostasis often become only apparent upon challenging with a high-fat diet. To explore whether *Ces1c/d/e*$^{-/-}$ mice will develop obesity-related metabolic disease, we fed mice a high-fat diet (HFD - 60% energy from fat) between 6 and 24 weeks of age, so for 18 weeks. *Ces1c/d/e*$^{-/-}$ female mice exhibited markedly higher body weights than the WT controls between 7 and 14 weeks, however, body weight curves then tended to merge between 15 and 24 weeks of age (Fig. S12A). We dissected the 24-week old mice and weighed different adipose tissues and organs. The weight of gWAT from *Ces1c/d/e*$^{-/-}$ compared to WT female mice was markedly decreased, and this was accompanied by severely increased inflammation, as evident from the marked infiltration of lymphocytes (Fig. S12B-C). However, iBAT from *Ces1c/d/e*$^{-/-}$ female mice was heavier than that of WT mice, and showed a clearly higher lipid load (Fig. S12B-C). Liver weights between both strains were similar but a pronounced fatty liver aspect was observed in mutant compared to WT female mice (Fig. S12B-C).

A parallel experiment was performed in males on a high-fat diet. From 6–12 weeks also *Ces1c/d/e*$^{-/-}$ male mice developed a higher body weight than WT mice. However, the body weight curves then merged over the next 3 weeks, and then the body weight trend even reversed, as shown by a lower body weight of mutant male mice compared to WT controls from 16 to 24 weeks (Fig. S13A). The weights of gWAT, mWAT and rWAT in 24-week old mutant compared to WT mice were markedly reduced, whereas iWAT weight was unchanged (Fig. S13B). In spite of these differences, both male strains showed similarly severe inflammation in gWAT, quite high lipid load in BAT and severe fatty liver (Fig. S13C). These results from the 18-week HFD study suggest that in females mutation of *Ces1c/d/e* can heavily disrupt lipid homeostasis in adipose tissues and liver compared with WT. However, they also show that treating FVB/NRj background male mice for 18 weeks with an HFD may perhaps overwhelm initial phenotypic differences caused by *Ces1c/d/e* deficiency.

As the initial body weight differences developed between 7 and 12 weeks of age, we designed a HFD experiment starting at 6, and

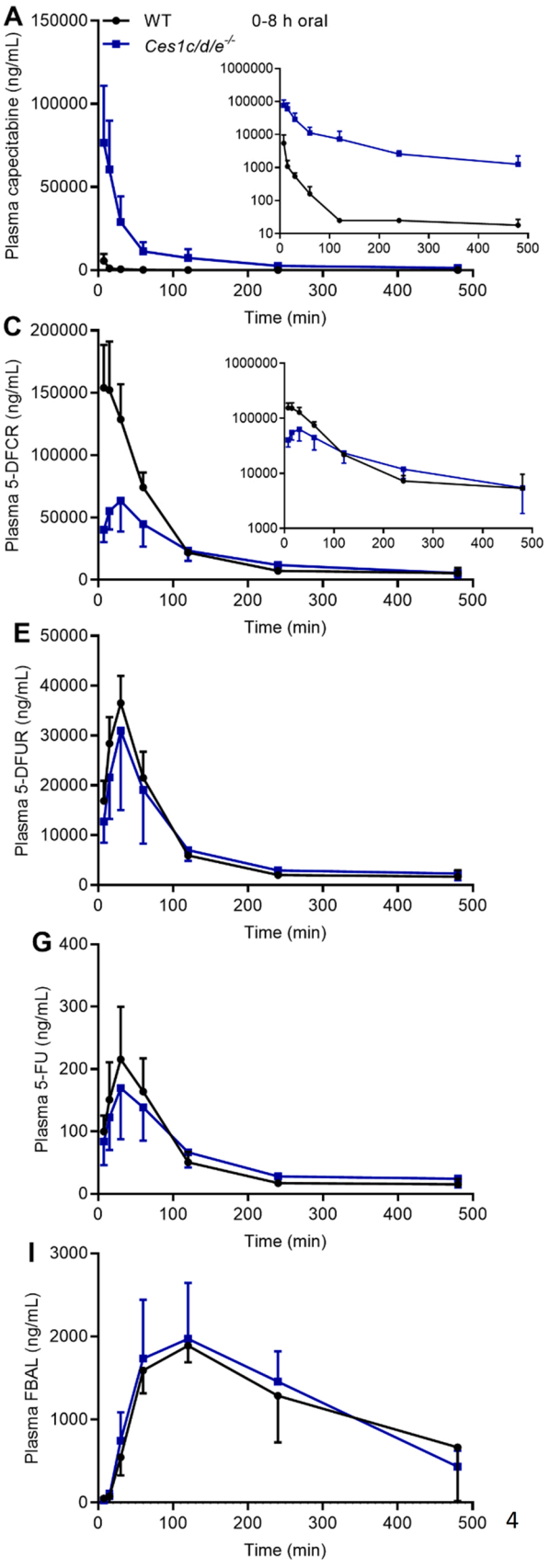

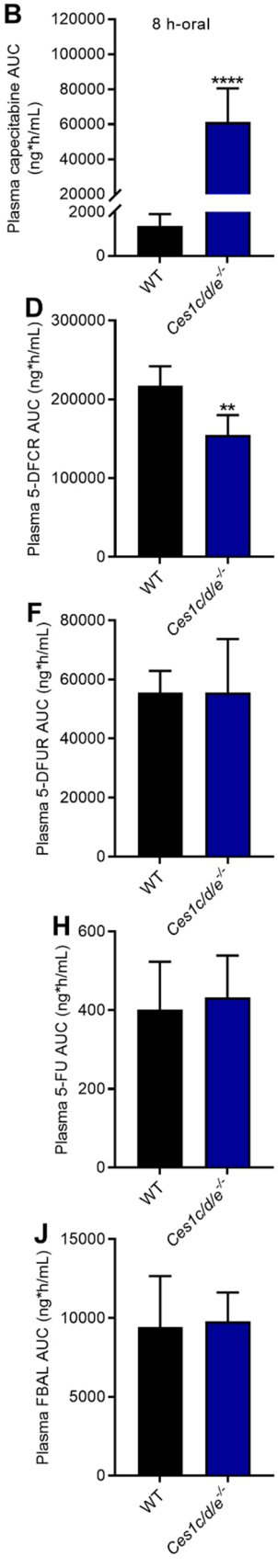

Fig. 4. Plasma concentrations and AUCs of capecitabine and related metabolites between WT and *Ces1c/d/e*$^{-/-}$ mice. Pharmacokinetics of capecitabine and its 4 metabolites (5-DFCR, 5-DFUR, 5-FU and FBAL) after oral administration of capecitabine (500 mg/kg) to female WT and *Ces1c/d/e*$^{-/-}$ mice. (A-B) Plasma capecitabine concentration versus time curves and AUCs. (C-D) Plasma 5-DFCR concentration versus time curves and AUCs. (E-F) Plasma 5-DFUR concentration versus time curves and AUCs. (G-H) Plasma 5-FU concentration versus time curves and AUCs. (I-J) Plasma FBAL concentration versus time curves and AUCs. Data are presented as mean ± SD ($n = 4$–5; $^{**}P < 0.01$; $^{****}P < 0.0001$ when compared with WT mice; the statistical calculation was performed after data were log-transformed; two-tailed unpaired Student's *t* test).

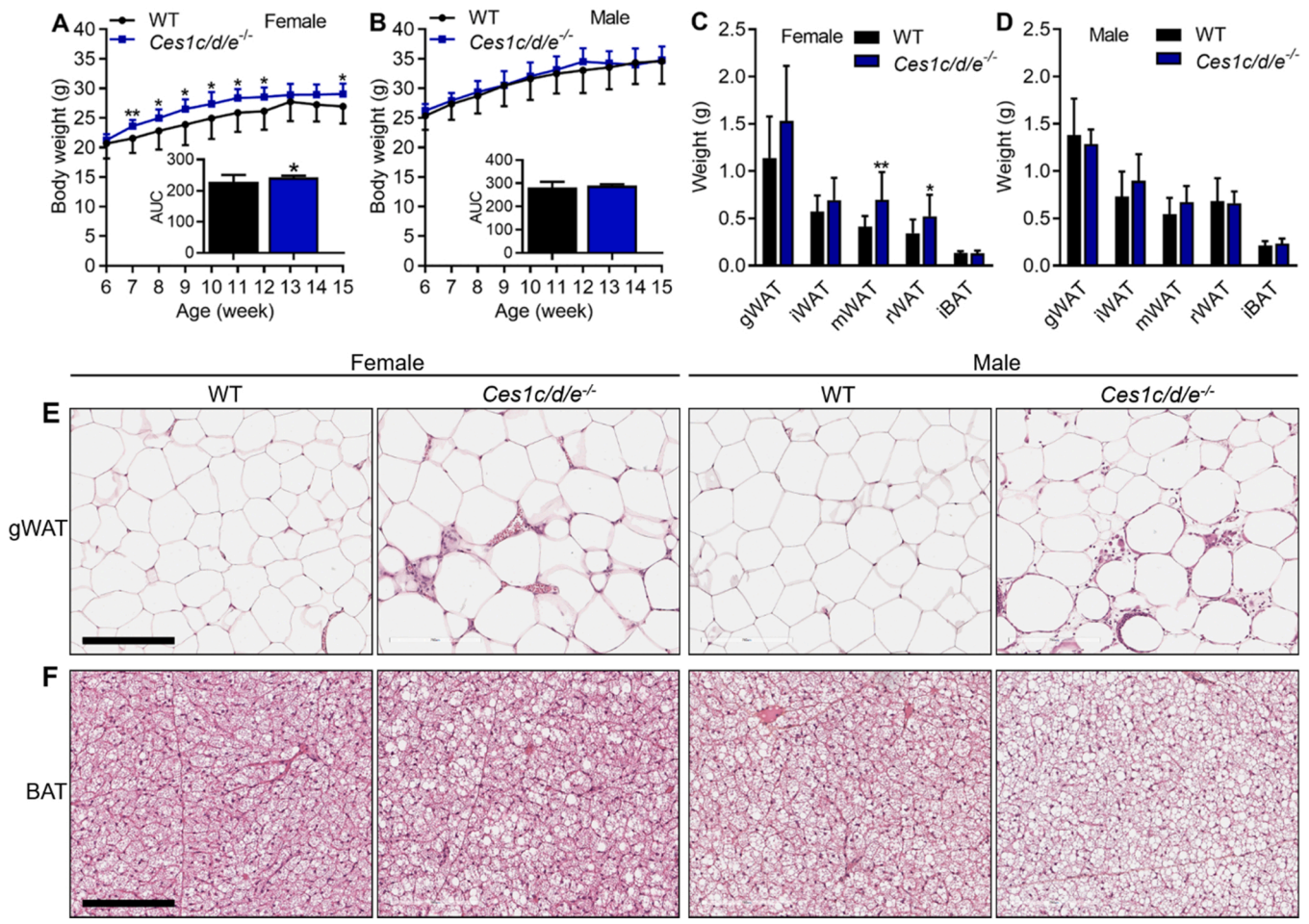

Fig. 5. *Ces1c/d/e*$^{-/-}$ mice display altered lipid homeostasis in adipose tissues under medium-fat diet. (A-B) Body weight development from 6 to 15 weeks of age (n = 9–16). (C-D) Weight of different adipose tissue depots (n = 11–12, 12–13 weeks). (E-F) Haematoxylin and eosin staining of perigonadal white adipose tissue (gWAT) and brown adipose tissue (BAT, n = 11–12, 12–13 weeks). Scale bars: 200 μm. Data are presented as mean ± SD (*P < 0.05; **P < 0.01 when compared with WT mice; two-tailed unpaired Student's t test).

terminating at 11 weeks of age, aiming to study the influence of *Ces1c/d/e* deficiency on lipid and glucose homeostasis in the phase where phenotypic differences emerged. At the end of this 5-week HFD exposure, *Ces1c/d/e*$^{-/-}$ female mice displayed higher body weights accompanied by heavier iWAT, mWAT and iBAT but reduced rWAT and unchanged gWAT (Fig. 6A, C). We also observed that the body weight of *Ces1c/d/e*$^{-/-}$ males increased faster than WT from 6 weeks of age, but at 11 weeks the statistical difference appeared to narrow down (Fig. 6B). These weight development profiles were very similar to what we previously observed in the 24-week HFD experiment (Fig. S13A). Like in females, iWAT, mWAT, and iBAT weights were increased, whereas rWAT, but in this case also gWAT, weights were decreased relative to WT controls (Fig. 6D). As shown in Fig. 6E, even upon general autopsy it was evident that gWAT of *Ces1c/d/e*$^{-/-}$ vs WT male mice was noticeably reduced. Apparent inflammation in gWAT was more severe in both female and male mutant than in WT mice (Fig. 6F), and this was further supported by upregulated expression of inflammatory markers such as TNF-alpha and F4/80 (Fig. 6G, H). Additionally, in male gWAT IL-6, IL-1b, and MCP1 were markedly upregulated, suggesting more advanced inflammation and possibly correlated with the reduced gWAT mass (Fig. 6D, G, H). The apparent lipid load in iBAT was also much higher in female and male *Ces1c/d/e*$^{-/-}$ mice, consistent with the increase in iBAT weight (Fig. 6C, D, and F).

Previous in vitro and in vivo work by another group has demonstrated that mouse Ces1d can stimulate glycerol and fatty acid release from adipocytes, thus impacting triglyceride mobilization [8]. Moreover, lower plasma glycerol and fatty acid levels were reported in *Ces1d* KO mice [9], suggesting that triglyceride mobilization in WAT is hampered when Ces1d is lacking. We also tested plasma levels of glycerol and fatty acid and found that in *Ces1c/d/e*$^{-/-}$ male mice these two parameters were clearly reduced compared with WT controls. However, in female mice we found no significant alteration in these parameters (Fig. 6I, J). It should be noted, however, that female mutant mice had overall markedly increased WAT mass (5.54 vs 4.36 g), whereas mutant male mice had roughly similar WAT mass compared to WT controls (4.67 vs 4.84 g, Fig. S14A). Normalized for the WAT mass, plasma glycerol and free fatty acid levels were therefore significantly decreased in the mutant strain in both sexes (except for the female plasma FFA to WAT mass ratio, P = 0.052, Fig. S14B-C).

3.6. *Ces1c/d/e mutation leads to fatty liver and type 2 diabetes in mice on a high-fat diet*

Nonalcoholic fatty liver disease (NAFLD) is closely associated with obesity [42,43]. In the 5-week HFD experiment, we noticed markedly heavier livers with pale appearance in *Ces1c/d/e*$^{-/-}$ mice when compared with WT (Fig. 7A, D). H&E and lipid staining (by Oil Red O) confirmed there was more lipid accumulation, and also in comparatively larger (but perhaps fewer) aggregates, in *Ces1c/d/e*$^{-/-}$ liver, especially in males (Fig. 7B, C). The total hepatic triglyceride mass was also higher than in WT, albeit with considerable variation (Fig. 7G). Plasma levels of two liver injury markers, alkaline phosphatase and alanine aminotransferase

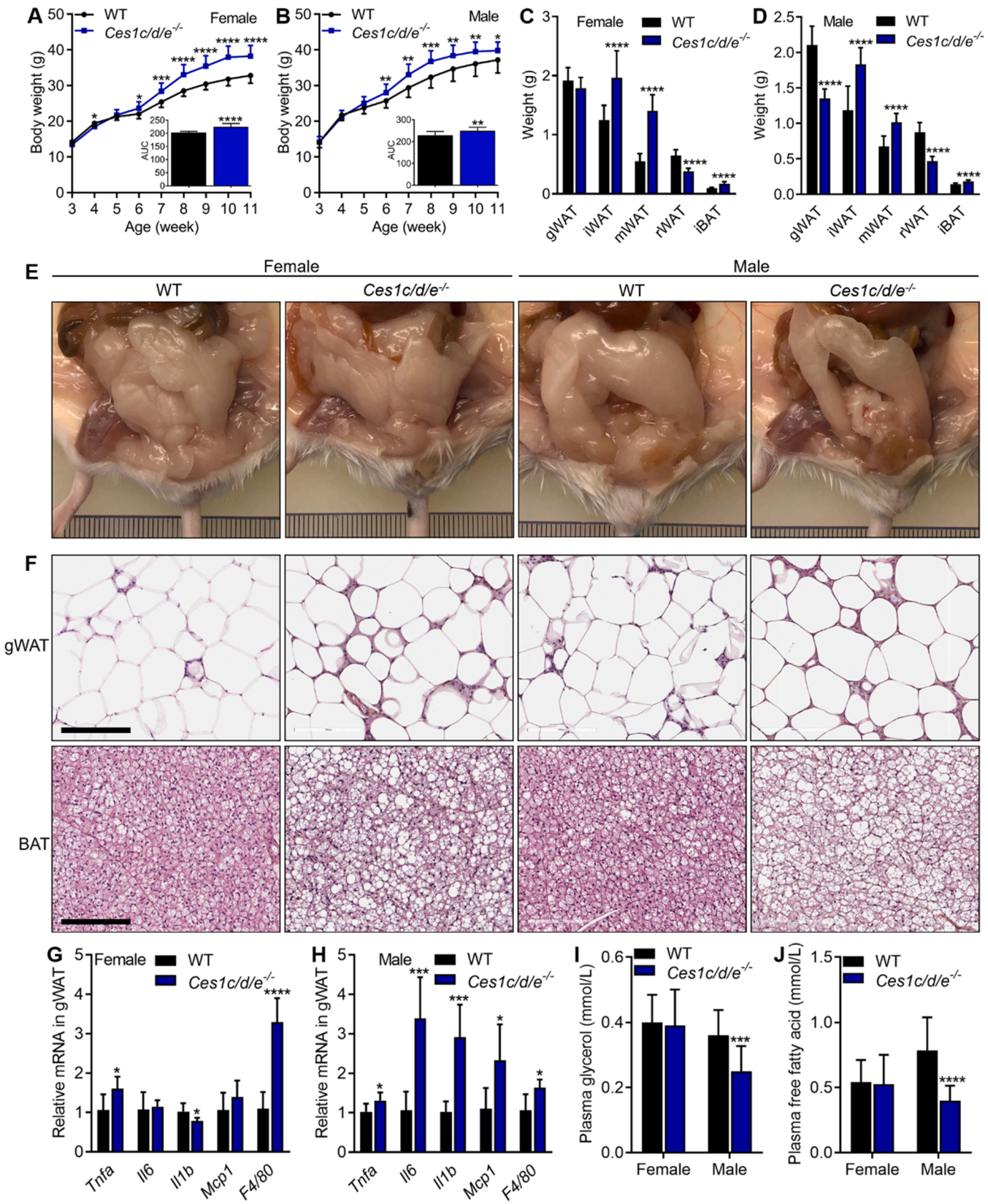

Fig. 6. *Ces1c/d/e*$^{-/-}$ mice develop obesity with severely disrupted lipid homeostasis after short-term treatment with a high-fat diet. Before 6 weeks, mice were treated with medium-fat diet. (A-B) Body weight development from 3 to 11 weeks of age (n = 13–16). (C-D) Weight of different adipose tissue depots (n = 13–16, 11 weeks). (E) Representative photos of perigonadal white adipose tissue (gWAT) of 11 week old mice (n = 7–15). (F) Haematoxylin and eosin staining of gWAT and brown adipose tissue (BAT, n = 13–16, 11 weeks). Scale bars: 200 μm. (G-H) Inflammatory gene expression checked by RT-qPCR in gWAT (n = 6, 11 weeks). (I-J) Glycerol and free fatty acids levels in plasma (n = 13–16, 11 weeks). Data are presented as mean ± SD (*P < 0.05; **P < 0.01; ***P < 0.001; ****P < 0.0001 when compared with WT mice; two-tailed unpaired Student's t test).

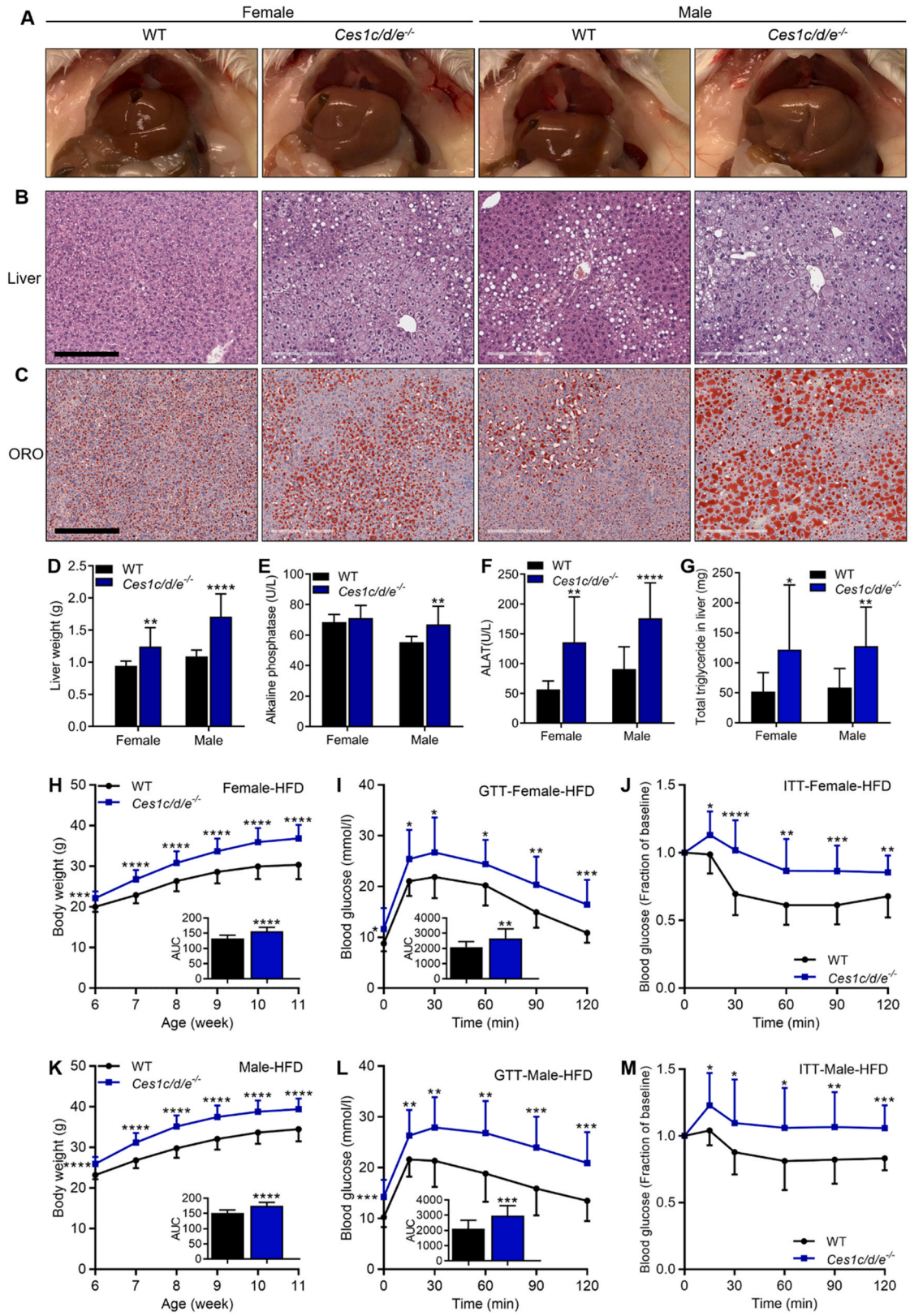

Fig. 7. *Ces1c/d/e*$^{-/-}$ mice develop liver steatosis, glucose intolerance and insulin resistance after short-term treatment with a high-fat diet. Before 6 weeks, mice were treated with medium-fat diet. (A) Representative photos of liver of 11-week old mice ($n = 7$–15). (B-C) Haematoxylin and eosin (top panels), Oil Red O (ORO, bottom panels) staining of liver ($n = 13$–16, 11 weeks). Scale bars: 200 μm. (D) Weight of liver ($n = 13$–16, 11 weeks). (E-F) Alkaline phosphatase and Alanine transaminase levels in plasma ($n = 13$–16, 11 weeks). (G) Triglyceride level in liver ($n = 13$–16, 11 weeks). (H-J) Body weight-time curves, glucose tolerance tests (11–12 weeks) and insulin tolerance tests (13–14 weeks) in females ($n = 15$–16) and males ($n = 13$–16) (K-M). Data are presented as mean ± SD (*$P < 0.05$; **$P < 0.01$; ***$P < 0.001$; ****$P < 0.0001$ when compared with WT mice; two-tailed unpaired Student's *t* test).

(ALAT), were also increased (except for alkaline phosphatase in females) (Fig. 7E and F). The liver is an important organ in regulating systemic lipid and glucose metabolism and can contribute to insulin resistance and type 2 diabetes development [44,45]. We therefore treated a different set of WT and *Ces1c/d/e*$^{-/-}$ mice with HFD from 6 weeks of age. These mice showed a similar profile of body weight development as we observed before (compare Fig. 6A, B; Fig. S12A, S13A; Fig. 7H, K). At 11 weeks of age, an oral glucose tolerance test was performed. *Ces1c/d/e*$^{-/-}$ mice could not efficiently reduce blood glucose after oral gavage, as evident from markedly higher blood glucose levels at all 6 time points in female and male mutant mice (Fig. 7I, L). Two weeks later, an insulin tolerance test was applied to the same mice. *Ces1c/d/e*$^{-/-}$ mice displayed strong insulin resistance compared with WT controls for both females and males (Fig. 7J, M and Fig. S15). Collectively, these are key hallmarks of type 2 diabetes [46,47]. These data demonstrate that, under high-fat diet conditions, mutation of mouse *Ces1c/d/e* can lead to early development of obesity-related metabolic disease, including fatty liver and type 2 diabetes.

To obtain a more general overview of molecular changes in the diet-challenged liver by the *Ces1c/d/e* mutation, we performed a hepatic proteomics analysis for mutant and WT mice at 11 weeks of age, after receiving a high-fat diet from week 6. In females, around 6000 proteins were detected of which ~150 displayed significantly different abundance between the strains (Fig. 8A). In male livers we also detected around 6000 proteins, of which ~250 showed statistically meaningful differences between the strains (Fig. 8B). We applied ingenuity pathway analysis (IPA: QIAGEN software) to explore which pathways were affected by *Ces1c/d/e* deficiency.

There was no obvious up- or downregulation of triglyceride biosynthetic enzymes, and this was supported by RT-PCR analysis (data not shown). Most of the top canonical pathways influenced were related to (xenobiotic) metabolism. *Ces1c/d/e*$^{-/-}$ female mice showed reduced metabolic pathway activities mainly caused by downregulated UDP-glucuronosyltransferase (UGT), sulfotransferase (SULT) and cytochrome P450 (CYP) enzymes. The acute phase response (APR) pathway closely followed these metabolic pathways and was strongly predicted to be activated based upon the IPA analysis: 7 proteins (MAPK8, SAA1, NFKB2, VWF, HPX, SERPINA1 and CFB) associated with APR were upregulated (Fig. 8A). Also in male *Ces1c/d/e*$^{-/-}$ mice SULT and CYP enzymes were enriched in the top canonical pathways (and predicted to be downregulated). The APR was also predicted to be activated in *Ces1c/d/e*$^{-/-}$ male mice compared with WT, with SAA1, HPX, C9, HP and CFB protein levels increased (Fig. 8B).

Taking the female and male proteomics data together, also since MAPK8 and NFKB2 are involved in metabolic inflammation [48,49], we analyzed the expression changes of 5 genes at the mRNA level (*Saa1*, *Hpx*, *Cfb*, *Mapk8* and *Nfkb2*). *Saa1* RNA was upregulated in *Ces1c/d/e*$^{-/-}$ female mice (Fig. 8C), whereas in mutant males *Saa1*, *Hpx* and *Nfkb2* showed higher expression levels (Fig. 8D). These findings support that *Ces1c/d/e* mutation in mice results in hepatic APR activation under HFD conditions. Recently, more evidence has emerged supporting that APR activation is not simply the response to cell injury, but also directly contributes to the progression of cancer [21], hepatitis [24] and other inflammatory diseases [19,20]. The likely role of APR activation in obesity-related metabolic disease development in *Ces1c/d/e*$^{-/-}$ mice will be further discussed below.

4. Discussion

Genetic drift is a main driver for evolution in nature [32], and it also often happens in laboratory animals [33,34]. However, it is not always straightforward to spot natural mutations in “wild-type” lab mouse

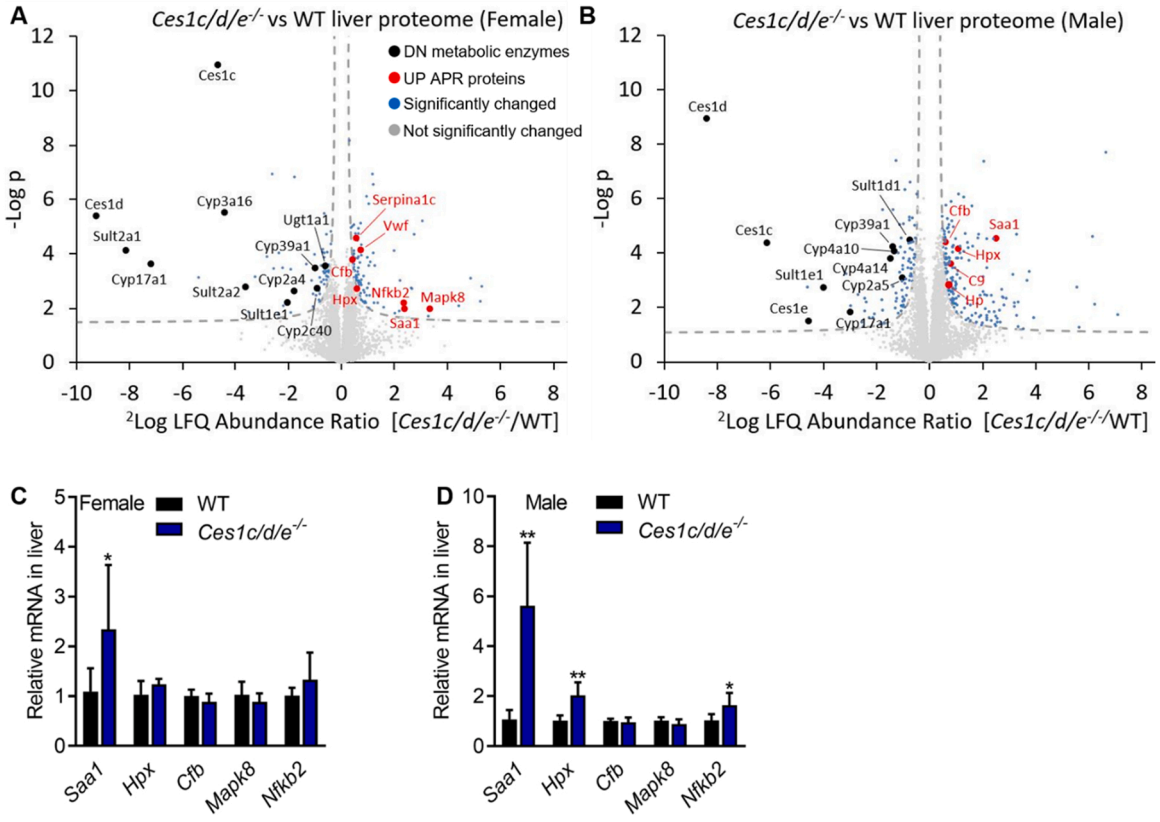

Fig. 8. Acute phase response (APR) is activated in liver of female and male *Ces1c/d/e*$^{-/-}$ mice after short-term treatment with a high-fat diet. Before 6 weeks, mice received a medium-fat diet. (A-B) Hepatic proteomics analysis ($n = 6$, 11 weeks). (C-D) RT-PCR analysis of gene expression in acute phase response signaling ($n = 6$, 11 weeks). Data are presented as mean ± SD (*$P < 0.05$; **$P < 0.01$ when compared with WT mice; two-tailed unpaired Student’s *t* test). DN: downregulated; UP: upregulated.

populations. In previous pharmacological studies with the immunosuppressive and anticancer drug everolimus, we observed either low or high, but no intermediate plasma levels of everolimus (with an approximately 50-fold difference) in a WT (FVB/NKI) population [7]. Through in vitro and in vivo experiments, we demonstrated that hepatic mRNA of *Ces1c*, *Ces1d*, and *Ces1e* was strongly upregulated in everolimus "high" WT compared with "low" WT mice, and that high plasma levels of Ces1c protein in the "high" mice could efficiently bind and retain everolimus, explaining the high plasma drug levels. Most WT mice had the "low" phenotype, and only a minority the "high" phenotype. Soon after, we observed similar behavior of the anticancer drug cabazitaxel, and arrived at similar conclusions [6].

Surprisingly, most knockout and transgenic strains for various other detoxifying genes we had previously generated behaved like the "high" everolimus/Ces1 mice, albeit with even 80-fold higher plasma levels than WT "low" mice and highly "upregulated" *Ces1c/d/e* expression. At the time we did not understand the cause of these expression differences [7]. However, it is now clear that "low" WT mice were homozygous for the *Ces1c/d/e* deletion, "high" WT mice heterozygous, and most previously generated knockout and transgenic strains homozygously proficient for *Ces1c/d/e*. The resulting changes in plasma Ces1c protein levels explain the differences in everolimus (and cabazitaxel) pharmacokinetic behavior. In the Methods section we present a reconstruction of how the different *Ces1c/d/e* genotypes emerged in our mouse strains.

This natural *Ces1c/d/e*$^{-/-}$ mouse model offered us an opportunity to explore Ces1c/d/e functions. In the pharmacokinetic study, conversion of irinotecan to its active metabolite SN-38 was noticeably reduced in plasma, spleen and lung after i.v. injection (Figs. 2, 3). However, the SN-38/irinotecan ratio was roughly similar in liver, kidney and small intestine between *Ces1c/d/e*$^{-/-}$ and WT mice (Fig. S2, S5), possibly reflecting the presence of alternative carboxylesterases (e.g., other Ces1 enzymes and Ces2) in these tissues. Perhaps related to this, irinotecan/SN-38-induced toxicity was not affected by loss of *Ces1c/d/e*. Both *Ces1c/d/e*$^{-/-}$ and WT mice exhibited similarly reduced white blood cells and thymus atrophy compared with untreated WT controls (Fig. S6).

The irinotecan/SN-38 pharmacokinetic experiments (8 h oral, 4 h i.v., 10 min i.v.) were performed simultaneously in WT, *Ces1c/d/e*$^{-/-}$ and *Ces1*$^{-/-}$ mice [31], allowing us to directly compare the impact of partial Ces1 family deletion (*Ces1c/d/e*$^{-/-}$) and whole Ces1 family knockout (*Ces1*$^{-/-}$). In each of these three independent experiments, we observed that the relative plasma exposure of SN-38 compared to irinotecan was lower in the *Ces1*$^{-/-}$ mice than in the *Ces1c/d/e*$^{-/-}$ mice, and much lower than in the WT mice, with mostly corresponding changes in the absolute irinotecan and SN-38 exposure levels (Fig. S16A-E). These results indicate that other Ces1 enzymes than the abundant plasma Ces1c can still noticeably affect the plasma levels of irinotecan and SN-38. Whether this happened by irinotecan conversion in plasma itself, or mostly in surrounding tissues (see below) is difficult to assess. Candidate enzymes are Ces1a, Ces1b, Ces1f and Ces1g, as Ces1h is not significantly expressed in liver or intestine (Supplemental Table 2).

In liver and kidney, the reduction in SN-38-to-irinotecan ratios in *Ces1*$^{-/-}$ compared to *Ces1c/d/e*$^{-/-}$ mice was more pronounced than in plasma, and even far more pronounced than the decrease between WT and *Ces1c/d/e*$^{-/-}$ mice (Fig. S17). This suggests that other Ces1 enzymes than Ces1c, d, and e play an important role in irinotecan metabolism in these tissues. In spleen, lung, and small intestine the shifts between the three strains were more intermediate (Fig. S18 and S19). Relatively higher expression of mouse *Ces1a*, *Ces1f* and *Ces1g* in liver and kidney than in spleen and lung might explain these differences [3], whereas spleen, lung and small intestine were perhaps more affected by the changes in plasma.

The pharmacokinetics of capecitabine and its 4 metabolites (5-DFCR, 5-DFUR, 5-FU and FBAL) was also investigated. All metabolite-to-capecitabine ratios in plasma were strongly reduced in *Ces1c/d/e*$^{-/-}$ mice (Fig. S8), but this was primarily because absolute plasma concentrations of capecitabine were massively increased, whereas its first metabolite 5-DFCR was somewhat decreased (Fig. 4). This is most likely because the plasma-localized Ces1c has a profound impact on the conversion of capecitabine to DFCR in plasma. In contrast, in most tissues we observed roughly similar levels of apparent capecitabine metabolism between these two mouse strains (Fig. S9). It is likely that in these tissues the other esterases have taken over capecitabine metabolism. Unlike for irinotecan, the in vivo pharmacokinetics of capecitabine and its 4 metabolites was very similar between *Ces1c/d/e*$^{-/-}$ and *Ces1*$^{-/-}$ mice (data not shown), probably again reflecting the major role for plasma Ces1c for this prodrug.

In the physiological study under medium-fat diet, lipid homeostasis was disrupted in *Ces1c/d/e*$^{-/-}$ mice, as shown by swollen adipocytes and inflammation in WAT and higher lipid load in BAT (Fig. 5E, F). However, overall body weight was not markedly altered. The medium-fat diet physiological experiments in *Ces1*$^{-/-}$ mice were performed simultaneously with those for *Ces1c/d/e*$^{-/-}$ mice (using the same WT controls). In general, the phenotypes we observed for these two *Ces1*-modified strains were quite comparable (body weight, tissue weight, adipose tissue and liver morphology) (data not shown). One difference was that we observed mild inflammation in WAT of female *Ces1c/d/e*$^{-/-}$ mice (Fig. 5E), which was absent in female *Ces1*$^{-/-}$ mice [31].

We therefore challenged the mice with a high-fat diet, aiming to explore whether loss of *Ces1c/d/e* will lead to obesity-related metabolic disease. Initially we designed an 18-week HFD (between 6 and 24 weeks of age) experiment. *Ces1c/d/e*$^{-/-}$ females at 24 weeks indeed exhibited more pronounced obesity-related pathological changes relative to WT females (more severe inflammation in WAT, higher lipid load in BAT and fatty liver), even though the initially higher body weights had converged at a later age with WT females (15–24 weeks, Fig. S12). gWAT and iWAT weights were significantly reduced, perhaps related to the inflammation. 18-week HFD results from males were more complicated. *Ces1c/d/e*$^{-/-}$ males initially (6–12 weeks) gained weight faster than WT, but they then slowed down and even showed a lower body weight than WT mice at a later age (16–24 weeks). This was accompanied by reduced gWAT, mWAT and rWAT weights, perhaps suggesting more progressive inflammation than in WT WAT (Fig. S13A, B). At 24 weeks, most pathological changes as assessed by HE staining in WAT, BAT and liver were roughly similar between *Ces1c/d/e*$^{-/-}$ and WT male mice, and about as severe as seen in female *Ces1c/d/e*$^{-/-}$ mice (Fig. S13C). It may be that male mice with an FVB/NRj genetic background are more sensitive to HFD challenge, and most phenotypic differences with WT caused by mouse *Ces1c/d/e* mutation are overwhelmed by long-term exposure to HFD.

After data analysis from the 24-week HFD study, we assessed that treating mice with HFD until 11 weeks (HFD between 6 and 11 weeks of age) would likely yield more informative phenotypic differences caused by *Ces1c/d/e* mutation. As shown in Fig. 6A-F, we observed obesity development and related pathological abnormalities in adipose tissues from *Ces1c/d/e*$^{-/-}$ female and male mice. Physiological roles of mouse *Ces1d* especially in lipid metabolism have been studied previously. As shown in vitro, the Ces1d enzyme participates in triglyceride hydrolysis in adipocytes, and knockdown of *Ces1d* can decrease fatty acid efflux from fat cells [8]. Moreover, *Ces1d* single KO mice showed reduced plasma levels of free fatty acids and glycerol compared with WT controls. Together, these observations suggested that mouse Ces1d can impact triglyceride mobilization. The lower plasma levels of free fatty acids and glycerol we observed in *Ces1c/d/e*$^{-/-}$ male mice suggested that normal triglyceride mobilization in WAT is hampered, causing over-accumulation of lipids and thus inflammation [50] (Fig. 6G-J).

In female mice, although the plasma levels of glycerol and free fatty acids were similar between *Ces1c/d/e*$^{-/-}$ and WT (Fig. 6I, J), the effectively increased overall WAT mass (unlike in males) meant that corrected for the WAT mass, plasma levels of glycerol and FFA were also decreased, like in males (Fig. S14A-C). Thus, in both male and female *Ces1c/d/e*$^{-/-}$ mice triglyceride mobilization in (and from) WAT may be compromised. The inflammatory effects (markers) in male WAT appear

more pronounced (compare Fig. 6G and H), possibly explaining the differences in overall WAT mass between the genders.

Clear fatty liver and type 2 diabetes phenotypes (glucose intolerance and insulin resistance) were also noted in *Ces1c/d/e*$^{-/-}$ mice on HFD (Fig. 7). It is obvious that lipid/glucose homeostasis at the whole body level was severely disrupted in this mutant mouse strain in the 11-week HFD study. We therefore decided to carry out a hepatic proteomics analysis on these HFD 11-week old mice, since liver is the key organ to distribute lipid/glucose to other organs (Fig. 8). Ingenuity pathway analysis (IPA: QIAGEN) of the proteomic data revealed that activity of several top canonical pathways in compound detoxification but also biosynthesis (like acetone degradation, heparan sulfate biosynthesis) was reduced by downregulating basic xenobiotic-metabolizing enzymes, like UDP-glucuronosyltransferase (UGT), sulfotransferase (SULT) and cytochrome P450 (CYP). It is well recognized that inflammation can downregulate UGT [51,52], SULT [53,54] and CYP [55–58] in liver.

Potentially increased inflammatory factors secreted by *Ces1c/d/e*$^{-/-}$ WAT may have accomplished this inter-organ cross-talk through blood [59–61]. Indeed, the acute phase response (APR) was strongly predicted to be activated based on IPA in HFD *Ces1c/d/e*$^{-/-}$ mice. The APR itself is an important component of the innate immune system. Upon different triggers (infection, cell injury, local/remote inflammation) the liver responds to recover physiological homeostasis by quickly producing many acute phase proteins (e.g., serum amyloid A, hemopexin and complement factors) [18]. Indeed, between female and male mice, we observed 9 typical APR upregulated proteins (MAPK8, SAA1, NFKB2, VWF, HPX, SERPINA1, C9, HP and CFB) in *Ces1c/d/e*$^{-/-}$ liver, although not always to the same extent between the genders. Albeit under medium-fat diet conditions, we also performed RNA-sequencing in liver and found that some molecules in the APR pathway were also upregulated in *Ces1c/d/e*$^{-/-}$ mice at the RNA level, like SAA1, C4, APCS, HPX, SERPINA1, C9 and HP in *Ces1c/d/e*$^{-/-}$ males; and SAA1, MAP2K6 and SERPINA1 in *Ces1c/d/e*$^{-/-}$ females (analyzed by IPA; data not shown and manuscript in preparation). This suggests that already under medium-fat diet conditions some level of APR activation in the liver had occurred.

Serum amyloid A1 attracted our attention since direct evidence from literature supports that SAA1 plays key roles in different inflammation-related diseases [19,20,24]. Since metabolic inflammation plays a key role in obesity-related metabolic disease [15,16], we hypothesize that SAA1 may contribute to the dynamic development of inflammation in *Ces1c/d/e*$^{-/-}$ mice, and thus impact obesity-related metabolic disease. In the medium-fat diet study, liver morphology and apparent triglyceride metabolism between WT and *Ces1c/d/e*$^{-/-}$ mice were still similar (Fig. S11). Yet, at the mRNA level, some APR related molecules were already clearly upregulated, especially SAA1. In the liver proteomics data from the high-fat diet study, SAA1 was also significantly increased in the *Ces1c/d/e*$^{-/-}$ mice (Fig. 8), coincident with fatty liver and type 2 diabetes. In this metabolic disease model, since SAA1 was already upregulated in the liver before morphological changes became apparent, it is therefore a potential candidate involved in the development of the systemic metabolic disease, and not just a secondary consequence of the overall changes in the liver, perhaps initially triggered by the primary inflammation in gWAT.

In this study, we identified and characterized a natural genomic deletion of the mouse *Ces1c/d/e* genes in an FVB(NKI) substrain previously considered wild-type. The in vivo pharmacokinetics of the anticancer prodrugs irinotecan and capecitabine was altered in this substrain. *Ces1c/d/e* deficiency disrupted lipid homeostasis, and *Ces1c/d/e*$^{-/-}$ mice were prone to developing obesity-related metabolic diseases, associated with an activated hepatic acute phase response under high-fat diet conditions.

Funding

This work was funded in part by the China Scholarship Council (CSC Scholarship No. 201506240145 to CPG). OBB and MA are supported by the Dutch NWO X-omics Initiative.

CRediT authorship contribution statement

Conceptualization: **Alfred H. Schinkel**, **Changpei Gan**; Methodology: **Alfred H. Schinkel**, **Changpei Gan**, **Alejandra Martínez-Chávez**, **Michel Hillebrand**, **Niels de Vries**, **Joke Beukers**, **Maria C. Lebre**, **Els Wagenaar**, **Hilde Rosing**, **Onno B. Bleijerveld**, **Maarten Altelaar**, **Jos H. Beijnen**; Investigation: **Changpei Gan, Jing Wang, Yaogeng Wang, Alejandra Martínez-Chávez, Michel Hillebrand, Niels de Vries, Joke Beukers, Els Wagenaar, Sjoerd Klarenbeek, Onno B. Bleijerveld, Ji-Ying Song**; Formal analysis: **Alfred H. Schinkel, Changpei Gan, Jing Wang, Onno B. Bleijerveld**; Data Curation: **Alfred H. Schinkel, Changpei Gan, Maria C. Lebre, Hilde Rosing**; Supervision: **Alfred H. Schinkel, Jos H. Beijnen**; Writing – original draft: **Alfred H. Schinkel, Changpei Gan**; Writing - Review & Editing: **Alfred H. Schinkel, Changpei Gan, Maria C. Lebre**; Resources: **Alfred H. Schinkel, Maria C. Lebre, Hilde Rosing, Maarten Altelaar, Jos H. Beijnen**. All authors reviewed and approved the final manuscript.

Declaration of Competing Interest

The authors declare that there are no conflicts of interest.

Data availability

Data will be made available on request.

Acknowledgments

We thank Marjolijn Mertz for assisting tissue slide scan; Bart van Wijnen and Enver Delic for clinical chemistry analysis; We also thank Slotervaart Medical Center for providing irinotecan hydrochloride trihydrate.

Appendix A. Supporting information

Supplementary data associated with this article can be found in the online version at doi:10.1016/j.biopha.2023.114956.

References

[1] L. Her, H.J. Zhu, Carboxylesterase 1 and precision pharmacotherapy: pharmacogenetics and nongenetic regulators, Drug Metab. Dispos. 48 (3) (2020) 230–244.
[2] J. Lian, R. Nelson, R. Lehner, Carboxylesterases in lipid metabolism: from mouse to human, Protein Cell 9 (2) (2018) 178–195.
[3] R.D. Jones, A.M. Taylor, E.Y. Tong, J.J. Repa, Carboxylesterases are uniquely expressed among tissues and regulated by nuclear hormone receptors in the mouse, Drug Metab. Dispos. 41 (1) (2013) 40–49.
[4] C.L. Morton, M. Wierdl, L. Oliver, M.K. Ma, M.K. Danks, C.F. Stewart, J.L. Eiseman, P.M. Potter, Activation of CPT-11 in mice: identification and analysis of a highly effective plasma esterase, Cancer Res. 60 (15) (2000) 4206–4210.
[5] C.L. Morton, L. Iacono, J.L. Hyatt, K.R. Taylor, P.J. Cheshire, P.J. Houghton, M. K. Danks, C.F. Stewart, P.M. Potter, Activation and antitumor activity of CPT-11 in plasma esterase-deficient mice, Cancer Chemother. Pharmacol. 56 (6) (2005) 629–636.
[6] S.C. Tang, A. Kort, K.L. Cheung, H. Rosing, T. Fukami, S. Durmus, E. Wagenaar, J. J. Hendrikx, M. Nakajima, B.J. van Vlijmen, J.H. Beijnen, A.H. Schinkel, P-glycoprotein, CYP3A, and plasma carboxylesterase determine brain disposition and oral availability of the novel taxane cabazitaxel (Jevtana) in mice, Mol. Pharm. 12 (10) (2015) 3714–3723.
[7] S.C. Tang, R.W. Sparidans, K.L. Cheung, T. Fukami, S. Durmus, E. Wagenaar, T. Yokoi, B.J. van Vlijmen, J.H. Beijnen, A.H. Schinkel, P-glycoprotein, CYP3A, and plasma carboxylesterase determine brain and blood disposition of the mTOR Inhibitor everolimus (Afinitor) in mice, Clin. Cancer Res. 20 (12) (2014) 3133–3145.
[8] E. Wei, W. Gao, R. Lehner, Attenuation of adipocyte triacylglycerol hydrolase activity decreases basal fatty acid efflux, J. Biol. Chem. 282 (11) (2007) 8027–8035.
[9] E. Wei, Y. Ben Ali, J. Lyon, H. Wang, R. Nelson, V.W. Dolinsky, J.R. Dyck, G. Mitchell, G.S. Korbutt, R. Lehner, Loss of TGH/Ces3 in mice decreases blood

lipids, improves glucose tolerance, and increases energy expenditure, Cell Metab. 11 (3) (2010) 183–193.
[10] J. Lian, E. Wei, S.P. Wang, A.D. Quiroga, L. Li, A. Di Pardo, J. van der Veen, S. Sipione, G.A. Mitchell, R. Lehner, Liver specific inactivation of carboxylesterase 3/triacylglycerol hydrolase decreases blood lipids without causing severe steatosis in mice, Hepatology 56 (6) (2012) 2154–2162.
[11] G. Li, X. Li, L. Yang, S. Wang, Y. Dai, B. Fekry, L. Veillon, L. Tan, R. Berdeaux, K. Eckel-Mahan, P.L. Lorenzi, Z. Zhao, R. Lehner, K. Sun, Adipose tissue-specific ablation of Ces1d causes metabolic dysregulation in mice, Life Sci. Alliance 5 (8) (2022).
[12] R. Schreiber, U. Taschler, H. Wolinski, A. Seper, S.N. Tamegger, M. Graf, S. D. Kohlwein, G. Haemmerle, R. Zimmermann, R. Zechner, A. Lass, Esterase 22 and beta-glucuronidase hydrolyze retinoids in mouse liver, J. Lipid Res. 50 (12) (2009) 2514–2523.
[13] E.A. Finkelstein, O.A. Khavjou, H. Thompson, J.G. Trogdon, L. Pan, B. Sherry, W. Dietz, Obesity and severe obesity forecasts through 2030, Am. J. Prev. Med. 42 (6) (2012) 563–570.
[14] V.S. Malik, W.C. Willet, F.B. Hu, Nearly a decade on - trends, risk factors and policy implications in global obesity, Nat. Rev. Endocrinol. 16 (11) (2020) 615–616.
[15] Y.S. Lee, J. Wollam, J.M. Olefsky, An Integrated View of Immunometabolism, Cell 172 (1–2) (2018) 22–40.
[16] G.S. Hotamisligil, Inflammation metaflammation and immunometabolic disorders, Nature 542 (7640) (2017) 177–185.
[17] J.R. Brestoff, D. Artis, Immune regulation of metabolic homeostasis in health and disease, Cell 161 (1) (2015) 146–160.
[18] C. Cray, J. Zaias, N.H. Altman, Acute phase response in animals: a review, Comp. Med. 59 (6) (2009) 517–526.
[19] J.Y. Lee, J.A. Hall, L. Kroehling, L. Wu, T. Najar, H.H. Nguyen, W.Y. Lin, S. T. Yeung, H.M. Silva, D. Li, A. Hine, P. Loke, D. Hudesman, J.C. Martin, E. Kenigsberg, M. Merad, K.M. Khanna, D.R. Littman, Serum amyloid a proteins induce pathogenic Th17 Cells and promote inflammatory disease, Cell 180 (1) (2020), 79-91.e16.
[20] U. Smole, N. Gour, J. Phelan, G. Hofer, C. Köhler, B. Kratzer, P.A. Tauber, X. Xiao, N. Yao, J. Dvorak, L. Caraballo, L. Puerta, S. Rosskopf, J. Chakir, E. Malle, A. P. Lane, W.F. Pickl, S. Lajoie, M. Wills-Karp, Serum amyloid A is a soluble pattern recognition receptor that drives type 2 immunity, Nat. Immunol. 21 (7) (2020) 756–765.
[21] J.W. Lee, M.L. Stone, P.M. Porrett, S.K. Thomas, C.A. Komar, J.H. Li, D. Delman, K. Graham, W.L. Gladney, X. Hua, T.A. Black, A.L. Chien, K.S. Majmundar, J. C. Thompson, S.S. Yee, M.H. O'Hara, C. Aggarwal, D. Xin, A. Shaked, M. Gao, D. Liu, M.J. Borad, R.K. Ramanathan, E.L. Carpenter, A. Ji, M.C. de Beer, F.C. de Beer, N.R. Webb, G.L. Beatty, Hepatocytes direct the formation of a pro-metastatic niche in the liver, Nature 567 (7747) (2019) 249–252.
[22] N. Venteclef, T. Jakobsson, K.R. Steffensen, E. Treuter, Metabolic nuclear receptor signaling and the inflammatory acute phase response, Trends Endocrinol. Metab. 22 (8) (2011) 333–343.
[23] R.Z. Yang, M.J. Lee, H. Hu, T.I. Pollin, A.S. Ryan, B.J. Nicklas, S. Snitker, R. B. Horenstein, K. Hull, N.H. Goldberg, A.P. Goldberg, A.R. Shuldiner, S.K. Fried, D. W. Gong, Acute-phase serum amyloid a: an inflammatory adipokine and potential link between obesity and its metabolic complications, PLoS Med. 3 (6) (2006), e287.
[24] Y.R. Ji, H.J. Kim, K.B. Bae, S. Lee, M.O. Kim, Z.Y. Ryoo, Hepatic serum amyloid A1 aggravates T cell-mediated hepatitis by inducing chemokines via Toll-like receptor 2 in mice, J. Biol. Chem. 290 (20) (2015) 12804–12811.
[25] A. Martínez-Chávez, H. Rosing, C. Gan, Y. Wang, A.H. Schinkel, J.H. Beijnen, Bioanalytical method for the simultaneous quantification of irinotecan and its active metabolite SN-38 in mouse plasma and tissue homogenates using HPLC-fluorescence, J. Chromatogr. B Anal. Technol. Biomed. Life Sci. 1149 (2020), 122177.
[26] L.D. Vainchtein, H. Rosing, J.H. Schellens, J.H. Beijnen, A new, validated HPLC-MS/MS method for the simultaneous determination of the anti-cancer agent capecitabine and its metabolites: 5'-deoxy-5-fluorocytidine, 5'-deoxy-5-fluorouridine, 5-fluorouracil and 5-fluorodihydrouracil, in human plasma, Biomed. Chromatogr. 24 (4) (2010) 374–386.
[27] D. Iusuf, M. Ludwig, A. Elbatsh, A. van Esch, E. van de Steeg, E. Wagenaar, M. van der Valk, F. Lin, O. van Tellingen, A.H. Schinkel, OATP1A/1B transporters affect irinotecan and SN-38 pharmacokinetics and carboxylesterase expression in knockout and humanized transgenic mice, Mol. Cancer Ther. 13 (2) (2014) 492–503.
[28] E. van de Steeg, C.M. van der Kruijssen, E. Wagenaar, J.E. Burggraaff, E. Mesman, K.E. Kenworthy, A.H. Schinkel, Methotrexate pharmacokinetics in transgenic mice with liver-specific expression of human organic anion-transporting polypeptide 1B1 (SLCO1B1), Drug Metab. Dispos. 37 (2) (2009) 277–281.
[29] V. Demichev, C.B. Messner, S.I. Vernardis, K.S. Lilley, M. Ralser, DIA-NN: neural networks and interference correction enable deep proteome coverage in high throughput, Nat. Methods 17 (1) (2020) 41–44.
[30] S. Tyanova, T. Temu, P. Sinitcyn, A. Carlson, M.Y. Hein, T. Geiger, M. Mann, J. Cox, The perseus computational platform for comprehensive analysis of (prote) omics data, Nat. Methods 13 (9) (2016) 731–740.
[31] C. Gan, J. Wang, A. Martínez-Chávez, M. Hillebrand, N. de Vries, J. Beukers, E. Wagenaar, Y. Wang, M.C. Lebre, H. Rosing, S. Klarenbeek, R.B. Ali, C. Pritchard, I. Huijbers, J.H. Beijnen, A.H. Schinkel, Carboxylesterase 1 family knockout alters drug disposition and lipid metabolism, Acta Pharm. Sin. B 13 (2) (2023) 618–631.
[32] R.D.H. Barrett, S. Laurent, R. Mallarino, S.P. Pfeifer, C.C.Y. Xu, M. Foll, K. Wakamatsu, J.S. Duke-Cohan, J.D. Jensen, H.E. Hoekstra, Linking a mutation to survival in wild mice, Science 363 (6426) (2019) 499–504.
[33] M.H. Shaw, V. Boyartchuk, S. Wong, M. Karaghiosoff, J. Ragimbeau, S. Pellegrini, M. Muller, W.F. Dietrich, G.S. Yap, A natural mutation in the Tyk2 pseudokinase domain underlies altered susceptibility of B10.Q/J mice to infection and autoimmunity, Proc. Natl. Acad. Sci. 100 (20) (2003) 11594–11599.
[34] S. Adriouch, C. Dox, V. Welge, M. Seman, F. Koch-Nolte, F. Haag, Cutting edge: a natural P451L mutation in the cytoplasmic domain impairs the function of the mouse P2X7 receptor, J. Immunol. 169 (8) (2002) 4108–4112.
[35] T. Satoh, M. Hosokawa, Structure, function and regulation of carboxylesterases, Chem. Biol. Inter. 162 (3) (2006) 195–211.
[36] R. Humerickhouse, K. Lohrbach, L. Li, W.F. Bosron, M.E. Dolan, Characterization of CPT-11 hydrolysis by human liver carboxylesterase isoforms hCE-1 and hCE-2, Cancer Res. 60 (5) (2000) 1189–1192.
[37] R.S. Holmes, M.W. Wright, S.J. Laulederkind, L.A. Cox, M. Hosokawa, T. Imai, S. Ishibashi, R. Lehner, M. Miyazaki, E.J. Perkins, P.M. Potter, M.R. Redinbo, J. Robert, T. Satoh, T. Yamashita, B. Yan, T. Yokoi, R. Zechner, L.J. Maltais, Recommended nomenclature for five mammalian carboxylesterase gene families: human, mouse, and rat genes and proteins, Mamm. Genome (21(9–10)) (2010) 427–441.
[38] F.M. de Man, A.K.L. Goey, R.H.N. van Schaik, R.H.J. Mathijssen, S. Bins, Individualization of Irinotecan treatment: a review of pharmacokinetics, pharmacodynamics, and pharmacogenetics, Clin. Pharm. 57 (10) (2018) 1229–1254.
[39] N.F. Smith, W.D. Figg, A. Sparreboom, Pharmacogenetics of irinotecan metabolism and transport: an update, Toxicol. Vitr. 20 (2) (2006) 163–175.
[40] S.K. Quinney, S.P. Sanghani, W.I. Davis, T.D. Hurley, Z. Sun, D.J. Murry, W. F. Bosron, Hydrolysis of capecitabine to 5'-deoxy-5-fluorocytidine by human carboxylesterases and inhibition by loperamide, J. Pharmacol. Exp. Ther. 313 (3) (2005) 1011–1016.
[41] J. Sanchez-Gurmaches, C.M. Hung, D.A. Guertin, Emerging complexities in adipocyte origins and identity, Trends Cell Biol. 26 (5) (2016) 313–326.
[42] J.P. Arab, M. Arrese, M. Trauner, Recent insights into the pathogenesis of nonalcoholic fatty liver disease, Annu Rev. Pathol. 13 (2018) 321–350.
[43] V.T. Samuel, G.I. Shulman, Nonalcoholic fatty liver disease as a nexus of metabolic and hepatic diseases, Cell Metab. 27 (1) (2018) 22–41.
[44] G. Targher, K.E. Corey, C.D. Byrne, M. Roden, The complex link between NAFLD and type 2 diabetes mellitus - mechanisms and treatments, Nat. Rev. Gastroenterol. Hepatol. 18 (9) (2021) 599–612.
[45] H. Tilg, A.R. Moschen, M. Roden, NAFLD and diabetes mellitus, Nat. Rev. Gastroenterol. Hepatol. 14 (1) (2017) 32–42.
[46] M. Roden, G.I. Shulman, The integrative biology of type 2 diabetes, Nature 576 (7785) (2019) 51–60.
[47] D.E. James, J. Stöckli, M.J. Birnbaum, The aetiology and molecular landscape of insulin resistance, Nat. Rev. Mol. Cell Biol. 22 (11) (2021) 751–771.
[48] J.M. Schattenberg, R. Singh, Y. Wang, J.H. Lefkowitch, R.M. Rigoli, P.E. Scherer, M.J. Czaja, JNK1 but not JNK2 promotes the development of steatohepatitis in mice, Hepatology 43 (1) (2006) 163–172.
[49] S.C. Sun, The non-canonical NF-κB pathway in immunity and inflammation, Nat. Rev. Immunol. 17 (9) (2017) 545–558.
[50] C.W. Liew, J. Boucher, J.K. Cheong, C. Vernochet, H.J. Koh, C. Mallol, K. Townsend, D. Langin, D. Kawamori, J. Hu, Y.H. Tseng, M.K. Hellerstein, S. R. Farmer, L. Goodyear, A. Doria, M. Blüher, S.I. Hsu, R.N. Kulkarni, Ablation of TRIP-Br2, a regulator of fat lipolysis, thermogenesis and oxidative metabolism, prevents diet-induced obesity and insulin resistance, Nat. Med. 19 (2) (2013) 217–226.
[51] T.A. Richardson, M. Sherman, D. Kalman, E.T. Morgan, Expression of UDP-glucuronosyltransferase isoform mRNAs during inflammation and infection in mouse liver and kidney, Drug Metab. Dispos. 34 (3) (2006) 351–353.
[52] M. Congiu, M.L. Mashford, J.L. Slavin, P.V. Desmond, UDP glucuronosyltransferase mRNA levels in human liver disease, Drug Metab. Dispos. 30 (2) (2002) 129–134.
[53] M.S. Kim, J. Shigenaga, A. Moser, C. Grunfeld, K.R. Feingold, Suppression of DHEA sulfotransferase (Sult2A1) during the acute-phase response, Am. J. Physiol. Endocrinol. Metab. 287 (4) (2004) E731–E738.
[54] S.I. Strasser, M.L. Mashford, P.V. Desmond, Regulation of uridine diphosphate glucuronosyltransferase during the acute-phase response, J. Gastroenterol. Hepatol. 13 (1) (1998) 88–94.
[55] E.T. Morgan, Impact of infectious and inflammatory disease on cytochrome P450-mediated drug metabolism and pharmacokinetics, Clin. Pharmacol. Ther. 85 (4) (2009) 434–438.
[56] A.E. Aitken, E.T. Morgan, Gene-specific effects of inflammatory cytokines on cytochrome P450 2C, 2B6 and 3A4 mRNA levels in human hepatocytes, Drug Metab. Dispos. 35 (9) (2007) 1687–1693.
[57] E.T. Morgan, Regulation of cytochrome p450 by inflammatory mediators: why and how, Drug Metab. Dispos. 29 (3) (2001) 207–212.
[58] E. Siewert, R. Bort, R. Kluge, P.C. Heinrich, J. Castell, R. Jover, Hepatic cytochrome P450 down-regulation during aseptic inflammation in the mouse is interleukin 6 dependent, Hepatology 32 (1) (2000) 49–55.
[59] C. Priest, P. Tontonoz, Inter-organ cross-talk in metabolic syndrome, Nat. Metab. 1 (12) (2019) 1177–1188.
[60] C.C. Duwaerts, J.J. Maher, Macronutrients and the adipose-liver axis in obesity and fatty liver, Cell Mol. Gastroenterol. Hepatol. 7 (4) (2019) 749–761.
[61] V. Azzu, M. Vacca, S. Virtue, M. Allison, A. Vidal-Puig, Adipose tissue-liver cross talk in the control of whole-body metabolism: implications in nonalcoholic fatty liver disease, Gastroenterology 158 (7) (2020) 1899–1912.